Sub-fossil chironomids as indicators of hydrological changes in the shallow and high-altitude lake Shen Co, Tibetan Plateau, over the past two centuries

Sonja Rigterink[1*], Paula Echeverría-Galindo[1], Rodrigo Martínez-Abarca[1], Julieta Massaferro[2], Philipp Hoelzmann[3], Bernd Wünnemann[3], Andreas Laug[1], Liseth Pérez[1], Wengang Kang[1], Nicole Börner[1], Anja Schwarz[1], Ping Peng[4], Junbo Wang[4], Liping Zhu[4], Antje Schwalb[1]

[1]Institute of Geosystems and Bioindication, Technische Universität Braunschweig, 38106 Braunschweig, Germany; [2]National Scientific and Technical Research Council of Argentina (CONICET), Bariloche, Argentina; [3]Institute of Geographical Sciences, Physical Geography, Freie Universität Berlin, 12249 Berlin, Germany; [4]Key Laboratory of Tibetan Environment Changes and Land Surface Processes, Institute of Tibetan Plateau Research, Chinese Academy of Sciences, Beijing, China

ABSTRACT

Understanding climate and monsoonal dynamics on the Tibetan Plateau is crucial, as recent hydrological changes, evidenced by rising lake levels, will be accelerated by current global warming and may alter aquatic habitats and species inventories. This study combines chironomid assemblages with sedimentological, mineralogical and geochemical data of a short sediment core (37.5 cm) from the high-altitude (>4,733 m asl), saline (9 g L^{-1}) and shallow (~5 m water depth) Shen Co, located in the southern part of the central Tibetan Plateau. The predominantly littoral, species-poor (10 chironomid morphotypes) chironomid assemblages are dominated by salt-tolerant taxa, that are highly sensitive to lake level fluctuations and macrophyte vegetation dynamics, making them ideally suited for tracking lake level changes over time. Results indicate a period (from ca. 1830 to 1921 CE) of drier conditions with low runoff and high evaporation rates in the Shen Co catchment, as indicated by a dominance of low-Mg calcite and dolomite and increased Ca/Fe and Sr/Rb ratios. This resulted in a decline in lake levels, an increase in salinity and the periodic occurrence of desiccation events at the sampling site. The first chironomid morphotype to appear after the dry period is *Acricotopus* indet. morphotype *incurvatus*, which indicate still low (<2 m) but rising lake levels after 1921 CE due to increasing runoff and a lower evaporation/precipitation ratio, as reflected by coarser grain size, higher quartz content and increased TN, TOC and Al/Si ratios. A replacement of *A.* indet. morphotype *incurvatus* by *Procladius* is observed as lake level rise continued after 1950 CE. The highest lake level is proposed for the period since 2006 CE. From 1955 to 1960 CE and from 2011 to 2018 CE, the presence of the phytophilic taxon *Psectrocladius sordidellus*-type supported abundant macrophyte growth. These changes are consistent with climate reconstructions from the northern and central Tibetan Plateau, indicating warmer and wetter climate conditions since the beginning of the 20th century, which have led to an increase in lake level in a number of Tibetan lakes. Our study specifically highlights 1920 and 1950 as years with enhanced precipitation. This can be attributed to strong overlapping multidecadal cycles of Westerlies and monsoon systems. This study demonstrates the significance of studying small, shallow lakes, as they frequently contain aquatic communities that respond more rapidly to the changes in the lake system. In addition, this study expands our understanding of the ecology of Tibetan chironomid morphotypes, highlighting this group's potential as paleolimnological proxies for investigating past environmental and climatic changes.

Corresponding author: s.rigterink@tu-braunschweig.de

Key words: Chironomidae; Asian summer monsoon; macrophytes; endorheic lake; Shen Co; Tibetan Plateau.

Citation: Rigterink S, Echeverría-Galindo P, Martínez-Abarca R, et al. Sub-fossil chironomids as indicators of hydrological changes in the shallow and high-altitude lake Shen Co, Tibetan Plateau, over the past two centuries. *J. Limnol. 2022;81:2077.*

Edited by: Diego Fontaneto, *CNR-IRSA Water Research Institute, Verbania, Italy.*

Received: 25 April 2022.
Accepted: 20 July 2022.

J. Limnol., 2022; 81:2077
DOI: 10.4081/jlimnol.2022.2077

INTRODUCTION

The Tibetan Plateau, also known as the "Water Tower of Asia", provides the majority of Asia's population with water from glaciers, rivers and lakes to a (Xu *et al.*, 2008). It is the highest plateau on Earth containing a large number of lakes (Zhang *et al.*, 2017a) that are extremely sensitive to environmental changes, such as temperature and lake level fluctuations, due to their relative isolation and largely undisturbed environments (Zhang *et al.*, 2017a). Numerous studies from the Tibetan Plateau have reported a continuous lake level rise in recent years, which has been attributed to increasing precipitation (Xu *et al.*, 2008; Lei *et al.*, 2013; Fang *et al.*, 2016) and enhanced glacial meltwater input

caused by global warming (Lu *et al.*, 2005; Zhang *et al.*, 2011; Zhou *et al.*, 2013; You *et al.*, 2016; Zhang *et al.*, 2017a). These observations point to a general trend towards warmer and wetter conditions in the region during recent decades (Yang *et al.*, 2011; Yang *et al.*, 2014a; Chen *et al.*, 2015; Zhang *et al.*, 2017b; Dong *et al.*, 2018; Wang *et al.*, 2018). Precipitation regimes on the Tibetan Plateau are directly dependent on the Asian summer monsoon (ASM) system (Morrill, 2004) and the Westerlies. The ASM, mainly consisting of the Indian (ISM) and East Asian summer monsoon (EASM), is an important component of the global climate system and responsible for the main precipitation on the Tibetan Plateau (Yao *et al.*, 2013). The dry climate in the winter months on the Tibetan Plateau is caused by the dominance of the mid-latitude Westerlies. When the Tibetan Plateau heats up in the summer months, between May and September, the ASM is responsible for increasing precipitation on the Tibetan Plateau (Yao *et al.*, 2013).

However, precipitation regimes on the Tibetan Plateau are highly variable in intensity, and changes in the monsoon systems are locally variable. For this reason, novel studies employing methods that provide direct statements about precipitation/evaporation are necessary to enhance our understanding of the factors that determine the precipitation patterns on the plateau.

Shallow, closed lakes in high mountain regions are sensitive to temperature and precipitation changes and lake level fluctuations (Lei *et al.*, 2014a), making them key ecosystems to study global climate and environmental variability (Nazarova *et al.*, 2011; Chang *et al.*, 2017; Wu *et al.*, 2020). Shallow lakes on the Tibetan Plateau are extreme habitats owing to their high salinities (Zhang *et al.*, 2007) and lake level variability, and they are commonly populated by organisms tolerant to these environmental conditions such as insects of the family of Chironomidae (Diptera). Chironomid larvae are one of the most abundant insect families in aquatic habitats (Ferrington, 2008) and can often still be used as paleolimnological proxies when other biological proxies (*e.g.*, diatoms) are no longer available due to poor conservation (Brooks *et al.*, 2007; Zhang *et al.*, 2007). Due to their excellent preservation in sediments (Walker, 1987), short life cycles and rapid response to climatic and environmental changes, their chitinous head capsules have been successfully used for decades as bioindicators to assess various environmental parameters such as air temperature, trophic state, salinity and changes in lake levels (Brooks, 2006). Because of their flying adults, chironomids reach a range of different habitats, quickly reacting to habitat changes. In arid and semi-arid areas like the Tibetan Plateau, salinity and lake level are the most important environmental variables, determining the chironomid distribution in this region (Zhang *et al.*, 2007). For this reason, chironomid assemblages in shallow lakes provide information about past humidity (evaporation/precipitation) and effective moisture (Chen *et al.*, 2009). Chironomid analyses have already been successfully used in several studies to reconstruct lake levels in China (Chen *et al.*, 2014) and effective moisture in Africa (Verschuren *et al.*, 2000a; Eggermont *et al.*, 2006), Canada (Heinrichs *et al.*, 2001; Heinrichs and Walker, 2006) and north-west China (Chen *et al.*, 2009).

Several studies show that the distribution of chironomid larvae in shallow lakes is also related to the presence of macrophytes and nutrient availability (Nazarova *et al.*, 2011; Greffard *et al.*, 2012; Tarkowska-Kukuryk, 2014; Zhang *et al.*, 2020). In recent decades, our understanding of the ecology of chironomids, particularly in high-altitude regions, has increased significantly. However, in remote regions such as the Tibetan Plateau, taxonomic and ecological knowledge of this insect group is still lacking (Zhang *et al.*, 2007; Zhang *et al.*, 2017c). Many specialized species that could serve as very good bioindicators are found on the Tibetan Plateau due to the heterogeneous landscape and habitat conditions. Chironomid morphotypes are still being found that cannot be attributed to any previously known chironomid species, but which could potentially become important for environmental reconstruction. An example is *A.* indet. morphotype *incurvatus*, so far endemic to the Tibetan Plateau, about which relatively little is known. *Acricotopus* indet morphotype *incurvatus* occurs in high abundances and in a variety of different habitats of the Tibetan Plateau such as in shallow ponds at Selin Co (Hamerlík *et al.*, 2010; Laug *et al.*, 2019), as well as in the saline Selin Co itself, or in the deep, freshwater Taro Co (Laug *et al.*, 2020a).

The aims of this study are:i)to produce the first high-resolution subfossil chironomid record for the shallow, high altitude Shen Co; ii) to assess which environmental variables shape the chironomid larvae community in Shen Co; iii) to reconstruct environmental changes based on subfossil chironomid larvae, geochemical, sedimentological and mineralogical data during the last 200 years; and iv) to compare the results of the chironomid analysis of Shen Co with paleoclimatic records from the Tibetan Plateau, including temperature and precipitation reconstructions (based on $\delta^{18}O$ of ice cores) and precipitation/evaporation data from the Tibetan Plateau, in order to identify possible links between the lake level variability of Shen Co and regional climate variability over the last 200 years.

Site description

Location and geology

Shen Co (Tibetan: Ser Tso) is a shallow (~5 m), high-altitude lake (4,733 m asl), situated in the southern part of the central Tibetan Plateau (30°59'51.75" N, 90°28'45.98" E, WGS84), Naqu region (Zhang *et al.*, 2021), with a lake area of ~52 km^2. The lake is located near Nam Co (Fig. 1a),

the second largest (~2,026 km^2) salt lake in China (Schütt *et al.*, 2010). The catchment area of Shen Co is 347.7 km^2 (Wang and Dou, 1998). The geology of the Shen Co basin consists mainly of Jurassic and Cretaceous clastic and carbonate rocks (Zhang *et al.*, 2008a), as well as quaternary alluvial sediments in the northern and eastern parts. The south-western part of the basin also contains carbonaceous arenite (Keil *et al.*, 2010; Yu *et al.*, 2021). The catchment is bordered by the ridge-and-valley landscape of the north-western hogbacks (elevations up to 5,400 m asl) of Nam Co (Keil *et al.*, 2010).

Climate and limnology

Shen Co is located in an endorheic basin. Unlike nearby lakes such as Nam Co, Shen Co does not receive any glacial

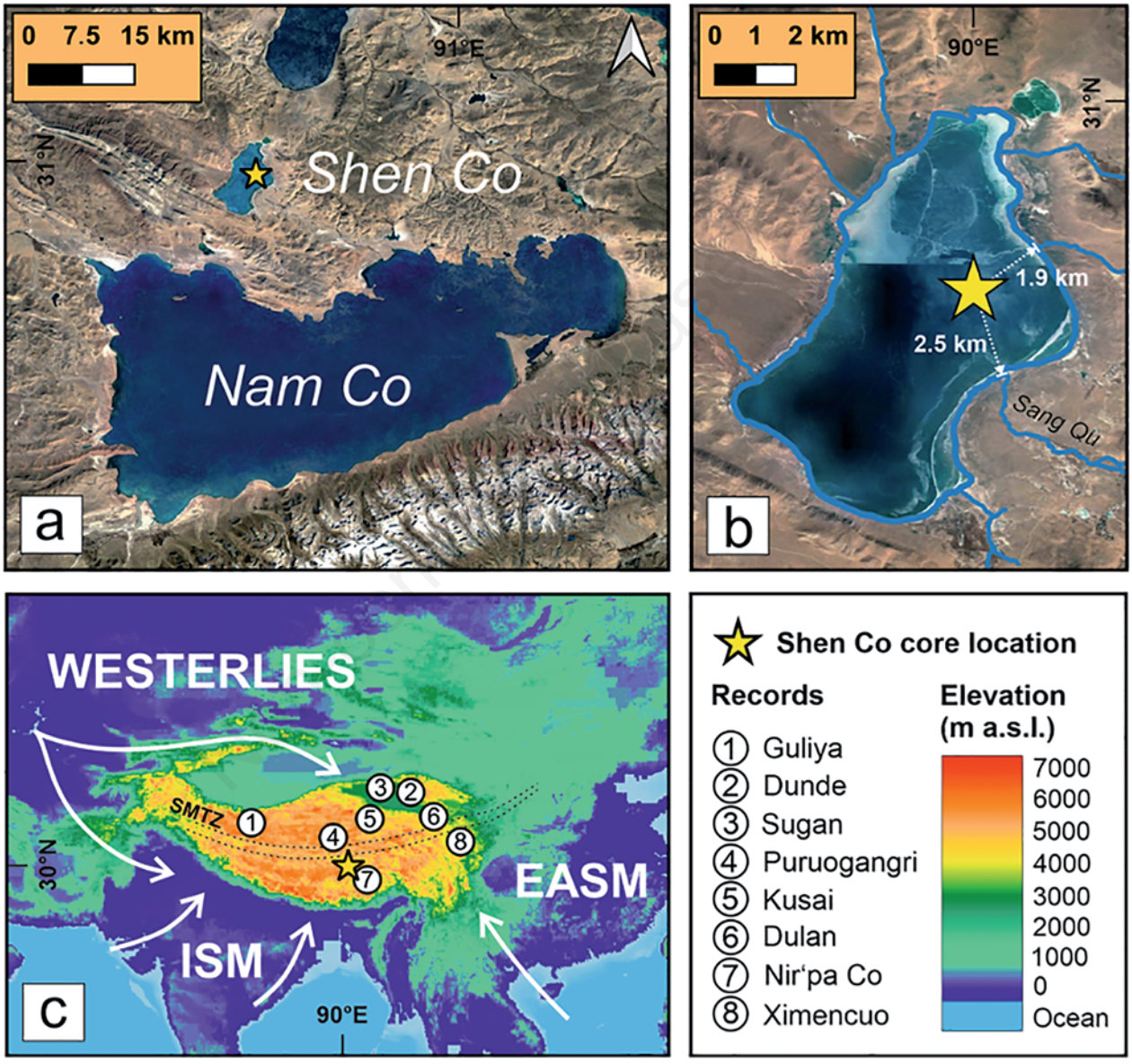

Fig. 1. a) Nam Co region. b) Shen Co core location (NC-18-40b). c) Atmospheric system over the Tibetan Plateau: Indian Summer Monsoon (ISM), the East Asian Summer Monsoon (EASM) and the Westerlies. The black dotted lines denote the Summer Monsoon Transition Zone (SMTZ) (after Wünnemann 2018). Circled numbers represent locations of different paleoclimate records from the Tibetan Plateau (Thompson *et al.*, 1989; Thompson *et al.*, 1997; Thompson *et al.*, 2006; Chen *et al.*, 2009; Pu *et al.*, 2013; Yang *et al.*, 2014b; Bird *et al.*, 2017; Cui *et al.*, 2021). Basemaps from Nam Co region and Shen Co were created with Google Satellite 2021, QGIS plugin. The World Digital Elevation Model (ETOPO1) used in this paper were provided by the European Environment Agency (https://www.eea.europa.eu/data-and-maps/data/world-digital-elevation-model-etopo5).

meltwater input, consequently the water balance is controlled only by precipitation and evaporation. Most of the water supply comes from rivers instead of groundwater (Wang and Dou, 1998). Currently, there are seven rivers draining into Shen Co (Fig. 1b), the most important one is Sang Qu (Wang and Dou, 1998), with a length of 21.5 km.

Shen Co was subject to a rise in lake area of 10-20% from 1970 until 2015 (Wan *et al.*, 2014; Zhang *et al.*, 2017a). Salinity decreased from 1997 until 2018. In 1997, a salinity of 23.51 g L^{-1} was measured in Shen Co (Wang and Dou, 1998). The present conductivity of the lake (17.97 mS cm^{-1} in July 2018) classifies Shen Co as mesohaline (8-30 mS cm^{-1}) (Bowman and Sachs, 2008) with a salinity of 9 g L^{-1}.

The region is characterized by semi-arid to sub-humid climate conditions (Wang *et al.*, 2011). Climatically, Shen Co is mainly influenced by the ISM, the mid-latitude Westerlies and the EASM (Fig. 1c) (Bolch *et al.*, 2010). The mean annual air temperature is -0.6°C (2007-2017) (Anslan *et al.*, 2020), the ice-covered period lasts from mid-January to late March (Cai *et al.*, 2019). The annual precipitation ranges between 291-568 mm (Anslan *et al.*, 2020). Most of the runoff into the lake occurs during the summer months (May to September), when precipitation reaches its maximum (Wrozyna *et al.*, 2010; Anslan *et al.*, 2020).

METHODS

Fieldwork

A 37.5 cm long sediment core NC-18-C-40b was retrieved in July 2018 using a UWITEC-piston corer at 4.8 m water depth. The coring site (31°0'58.72" N, 90°30'0.76" E) was 1.9 km far from the east-shoreline, 2.5 km from the closest inflow Sang Qu (Fig. 1b). During field work in July 2018, different limnological parameters were measured:Oxygen saturation, pH, surface water temperature and alkalinity.

Laboratory work

Lithological description

The sediment core was split lengthwise. The cut face was cleaned with a glass slide and distilled water and imaged using a Canon camera. Sediment description was done by visual inspection of the cleaned sediment surface. The stratigraphic description was carried out considering grain size, sedimentary structures, color, macroscopic components (*e.g.*, roots, charcoal) and type of boundary. Sediment color was determined by using Munsell Soil Color Chart (Munsell Color, 2010). The stratigraphic column was made in the free distribution software SedLog 3.1 (Zervas *et al.*, 2009). Microscopic smear-slide analysis was conducted to make a semi-quantitative analysis of the major components as well as texture and sorting following Schnurrenberger *et al.* (2003).

Chronology

Dried sediment samples of the uppermost 20 cm were analyzed at 1 cm intervals for 210-Lead (^{210}Pb), 226-Radium (^{226}Ra), 137-Cesium (^{137}Cs) and 241-Amaritium (^{241}Am). Measurements were carried out with an ORTEC HPGe GWL series well-type coaxial low background intrinsic germanium detector at the Environmental Radiometric Facility at University College London. ^{210}Pb was determined via its gamma emissions at 46.5keV, and ^{226}Ra at 295 keV and 352 keV gamma rays emitted by its daughter isotope ^{214}Pb following three weeks storage in sealed containers to allow radioactive equilibration. ^{137}Cs and ^{241}Am were measured by their emissions at 662keV and 59.5keV (Appleby *et al.*, 1986). The absolute efficiencies of the detector were determined using calibrated sources and sediment samples of known activity. Corrections were made for the effect of self-absorption of low energy gamma rays within the sample energy gamma rays within the sample using Constant Rate of Supply (CRS) Model (Appleby *et al.*, 1992). In addition, three bulk sediment samples were used for ^{14}C dating at Beta Analytic (Miami, FL, USA). ^{14}C dates were calibrated using IntCal 20 (northern hemisphere) calibration (Reimer *et al.*, 2020). The linear age-depth model was built using Calib 8.1.0 (Reimer *et al.*, 2013). All ages are expressed in calendar years (CE hereafter).

Geochemical analysis

Sub-samples were collected at 2 cm intervals, oven dried at 50ºC for 24 h, and grounded to a fine powder. Major elemental analyses, total carbon (TC), total inorganic carbon (TIC), and total nitrogen (TN) were analyzed at the Institute of Geographical Science at the Freie Universität Berlin, Germany. For elemental analyses, dry powdery samples were placed into plastic cups, sealed with a mylar foil (0.4 µm) and analyzed with a portable energy-dispersive X-ray fluorescence spectrometer (P-ED XRF) Analyticon NITON XL3t. LKSD-2 and LKSD-4 were used as certified reference material to verify the recovery values for the elements detected by p-ED-XRF. All XRF element ratios were calculated as element molar ratios. TC and TN were determined with a LECO TruSpec CHN-analyzer by combustion of 100 mg of dried samples (at 105°C) in an O_2 stream at 950°C and CO_2-detection by IR spectroscopy and thermal conductivity measurement. A Wösthoff Carmhograph C-16 was used to determine TIC after evolving CO_2 from 100 mg of the dried sample by adding 42.5 H_3PO_4. The evolved CO_2 produced a change of conductivity in NaOH representative to the TIC content

of the sample. Total organic carbon (TOC) was calculated by subtracting TIC from TC. TOC and TN were used to calculate the C/N molar ratio for those samples that showed TOC values >0.7%.

Mineralogy

We carried out a semi-quantitative analysis of the mineralogical compounds by X-ray powder diffraction (XRD). A RIGAKU Miniflex600 diffractometer was used at 15 mA/40 kV (Cu kα) from 3° to 80° (2θ) with a goniometer step velocity of 0.02° steps and 0.5° min^{-1}. We used the software Match! Version 3.11.5.203 (Dr. H. Putz & Dr. K. Brandenburg GbR) for semi-quantitatively identifying the mineral composition. Within this program outliers were corrected, the kα2-Peaks were eliminated, and the 2° angles were calibrated to the main quartz peak with an intensity of 100 main peak (d=3.34 Å). We established a reference mineralogical dataset composed by the major expected minerals (carbonates, silicates and oxides) according with the regional geology (Zhang *et al.*, 2008a; Keil *et al.*, 2010; Yu *et al.*, 2021). Crystallographic Information Files (CIF) for the reference dataset. as well as the reference intensity ratio (RIR) to make the semiquantitative analysis, were obtained from The American Mineralogist Crystal Structure Database (Downs and Hall-Wallace, 2003). The XRD-results are expressed in relative percentage (%).

Chironomidae analysis

Sub-samples were collected at 0.5 cm intervals throughout the core. Sediment samples were freeze-dried (ca. -60°C) for 24-36 h to calculate dry mass (water content). Samples were prepared with potassium hydroxide solution (10%) and heated for 20 minutes at 80-90°C (Walker, 1987). The deflocculated sediment was passed through a 100 µm mesh nylon sieve. Head capsules were hand-picked under a stereo-zoom microscope at 32 and 16 × magnification. The statistic relevant minimum number of head capsules was 50 per sample (Larocque, 2001). Identification of chironomid taxa was done using a Zeiss Axio ImagerA2 microscope following Brooks *et al.* (2007) and Bitušík and Hamerlík (2014). Chironomid head capsules were determined to the highest possible taxonomic resolution, mostly morphotypes. Head capsule concentrations are presented as number of head capsules per dry mass sediment (head capsules g^{-1}).

A. indet. morphotype *incurvatus* and *Acricotopus* type K were the only determined morphotypes that are not present in the identification literature. Identification of both morphotypes followed Laug *et al.* (2018, 2019). Characteristics of *A.* indet. morphotype *incurvatus* head capsule are a mentum with three median teeth and eight lateral teeth, all arranged on a different focal plane than median teeth. Plate behind mentum is visible on some individuals. The mandible has four inner teeth. *A.* type K differs from *A.* indet. morphotype *incurvatus* by lateral teeth clumped and on a different focal plane (Laug *et al.*, 2018).

Statistical analysis

Graphical representation of Chironomidae total abundances was done with the program C2, Version 1.7.7. (Juggins, 2014). Chironomid morphotypes which occurred with a maximum abundance of ≤2% were eliminated from the analysis. Total chironomid abundances were used for all statistical analysis. Chironomid abundances were square-root transformed prior to ordination and cluster analyses. Environmental variables were standardized and transformed using *decostand* (Anderson *et al.*, 2006). Stratigraphic zones of the chironomid assemblages as well as geochemical and mineralogical data were defined using constrained hierarchical cluster analysis with Bray–Curtis distance and CONISS linkage method (Grimm, 1987). The statistical significance of the clusters were assessed using a broken-stick model (Bennett, 1996). Diversity was calculated by Shannon index to determine taxon richness of the chironomid assemblage data. Principal Components Analysis (PCA) was used to explore the major gradients in chironomid assemblages in relation to the environmental variables. Detrended Correspondence Analysis (DCA) was used to estimate the amount of chironomid compositional change within the data as well as to identify the gradient length within the chironomid data to determine whether linear or unimodal based numerical techniques should be used (Hill and Gauch, 1980). Variance inflation factors (VIF) were calculated to identify and exclude non-linear independent variables from the analysis (Miles, 2014). The significance of each variable was tested using a variance analysis (ANOVA) (999 permutations). All analyses were performed using *vegan*-package and *rioja*-package from R software (R Core Team, 2019).

Landsat imagery

Lake boundaries from Shen Co as well as islands in the lake were generated from Landsat images acquired by TM/ETM+ using QGIS. The data sets used include Landsat satellite images from 1973-2021, only images that were taken during the summer months and had a cloud cover of <10% were considered. Landsat scenes had a spatial resolution of 30 m (Williams *et al.*, 2006; Wulder *et al.*, 2019). Surface area of the temporal scenes were calculated using QGIS. Landsat satellite images from Shen Co are available from the website of the United States Geological Survey (https://www.usgs.gov/).

RESULTS

Fieldwork

During field work in July 2018, the following water parameters (Suppl. 1) were measured:the bottom of the lake was well-oxygenized (5.82 mg L^{-1} or 103.4 %), the pH was alkaline (9.5) with a 15°C surface water temperature and a 201 mmol L^{-1} alkalinity.

Chronology – Age model

The age-depth model for the sedimentary record NC-18-40b was constructed using ^{210}Pb and ^{137}Cs and ^{241}Am activities (Fig. 2a, Suppl. 2a). The fixed age in the ^{210}Pb/^{137}Cs model are based on the zero value for Cs at 14 cm depth (=1950 or 1952 CE), this is also supported by a first peak of ^{241}Am. The 1963 CE peak of ^{137}Cs (highest nuclear fallout) is visible but is set where the Cs values show a slight first peak upward (10.75 cm). A further pronounced peak occurs at 3 cm depth and probably represents the Chernobyl nuclear outfall in 1986 CE. This also corresponds to the calculated sediment accumulation rates (SAR) of 0.195 cm yr^{-1} from 0 to 11.5 cm and 0.230 cm yr^{-1} from 12 to 16 cm (Suppl. 2b). For the bottom part of the core (16 to 37.5 cm) SAR are not available, but we assume constant sedimentation accumulation rates for the bottom part of the core, especially until the clay sections turns to a siltier substrate at around 21 cm. Hiatuses were excluded due to the homogenous sedimentology of the sediment core until 21 cm depth, for this reason, we extrapolated the ^{210}Pb-^{137}Cs data with constant sedimentation rates until 21 cm. For the rest of the core, the age model is unclear (Fig. 2b, grey line/scatter plot) but we assume a linear age model until 37.5 cm. Missing values were calculated using linear regression (Suppl. 2c).

Four radiocarbon ages at 2.5 cm, 18.5 cm, 22.5 cm and 36 cm depth (Suppl. 2d) yielded remarkably older ages compared with the calculated radionuclide (Pb/Cs) ages and thus indicating reservoir errors of 1594 years (2.5 cm

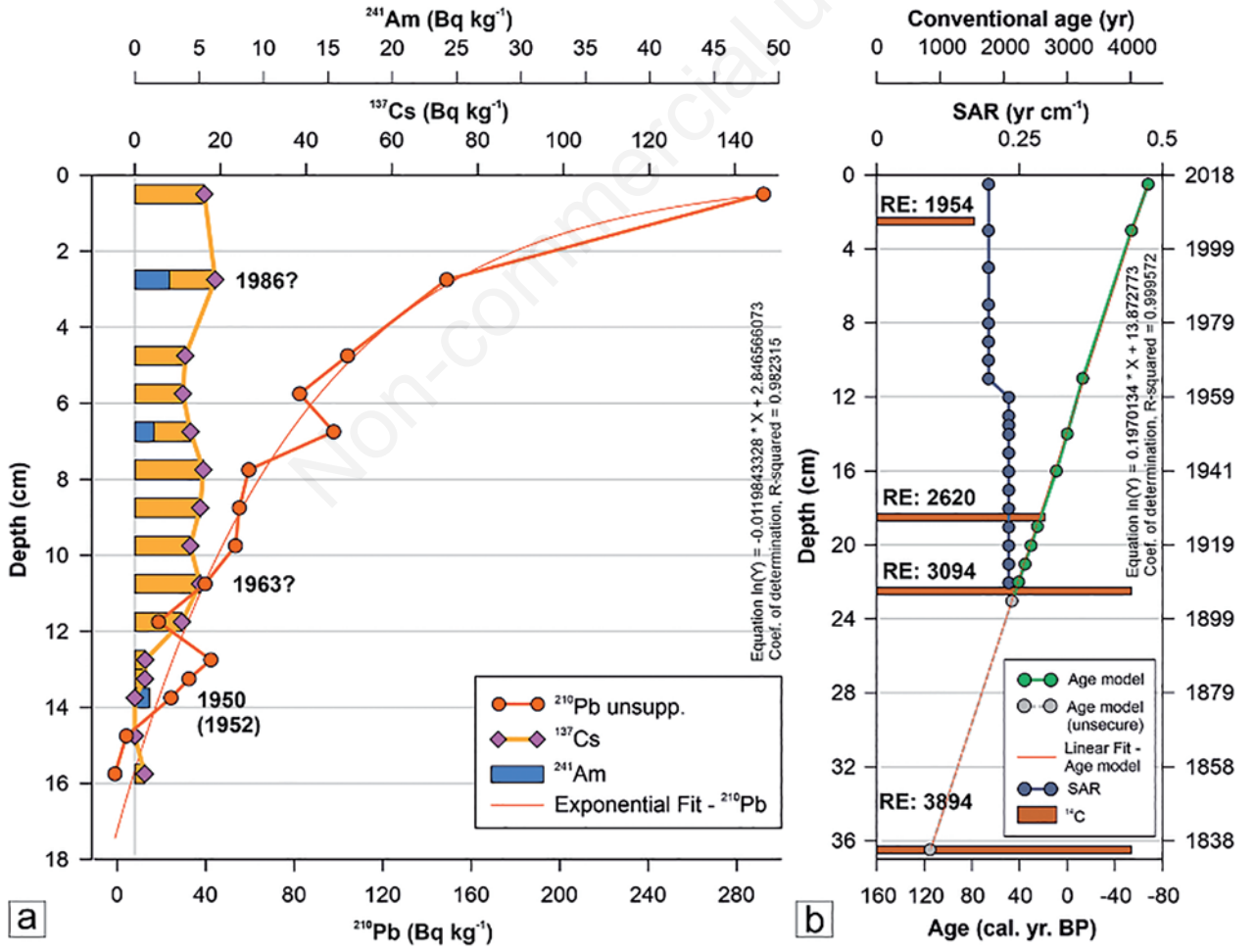

Fig. 2. Activity of ^{137}Cs, ^{210}Pb and ^{241}Am (a), age-depth correlation (b) of the Shen Co sediment short core NC18-40b (dottet, green line), sediment accumulation rates (SAR) (dotted, grey line) and ^{14}C ages (brown bars). RE denoted for reservoir effect.

depth) and even 3894 years (36 cm depth), likely due to old carbon supply by river transport from the nearby catchments. Calibration (Suppl. 2e) was only made for the last ^{14}C age using IntCal20, which shows only slight differences to the ^{210}Pb-^{137}Cs data.

Stratigraphy and lithology

Three sedimentary units were identified along the core sequence (Fig. 3, Suppl. 3). The oldest unit ranging from 37.5 to 21 cm is characterized by an alternation of massive yellowish silt (Hue 10 YR 7/6) with 1 cm-thick dark fine sand deposits. The latter are composed of well sorted, sub-rounded to rounded calcite grains and feldspar and pyroxenes in lower abundances. Dark sediments are characterized by gradual basal contacts and erosive upper boundaries. A massive, organic-rich clay layer lies between 34.5 and 32.5 cm. This yellowish to olive layer (Hue 5 YR 5/4) is rich in well-preserved aquatic plant fragments. The second unit stretches from 21 to 17 cm and begins with an erosive boundary overlain by clay with laminated fine sand layers. The third unit reaches from 17 to 0 cm. It consists of a massive, pale yellow, organic-rich clay (Hue 2.5 YR 8/3) with a high content of aquatic plant fragments.

Mineralogy and geochemistry

In general, the mineralogical composition (Fig. 3, Suppl. 4a) of the sediments consists of carbonates (low-Mg calcite, dolomite), quartz, micas (biotite, muscovite), silicates (vermiculite, montmorillonite, illite), feldspar and plagioclase (albite, orthoclase), and oxides like magnetite. Total organic carbon (TOC), Total Nitrogen (TN) as well as Carbon/Nitrogen (C/N), Aluminum/Silicium (Al/Si), Calcium/Iron (Ca/Fe) and Strontium/Rubidium (Sr/Rb) ratios are shown as geochemical parameters (Fig. 3, Suppl. 4b). Mineralogy and geochemistry were categorized in three zones according to Constrained Clustering (Suppl. 4c).

Zone I (37.5-24.5 cm = ~1831-1896 CE)

The bottom part of the core is dominated by low-Mg calcite with values up to 63 %, quartz (~20%), dolomite (up to 18%) and biotite (up to 12%) as well as low percentages (<5%) of montmorillonite and magnetite. The lowest TOC values of the core (0.15-3.24%) were measured in this zone. The maximum TOC value is reached in the upper part of this zone (24.5 cm). TIC ranges from 5.64-7.09%. TN values range from 0.09-0.18%, the lowest

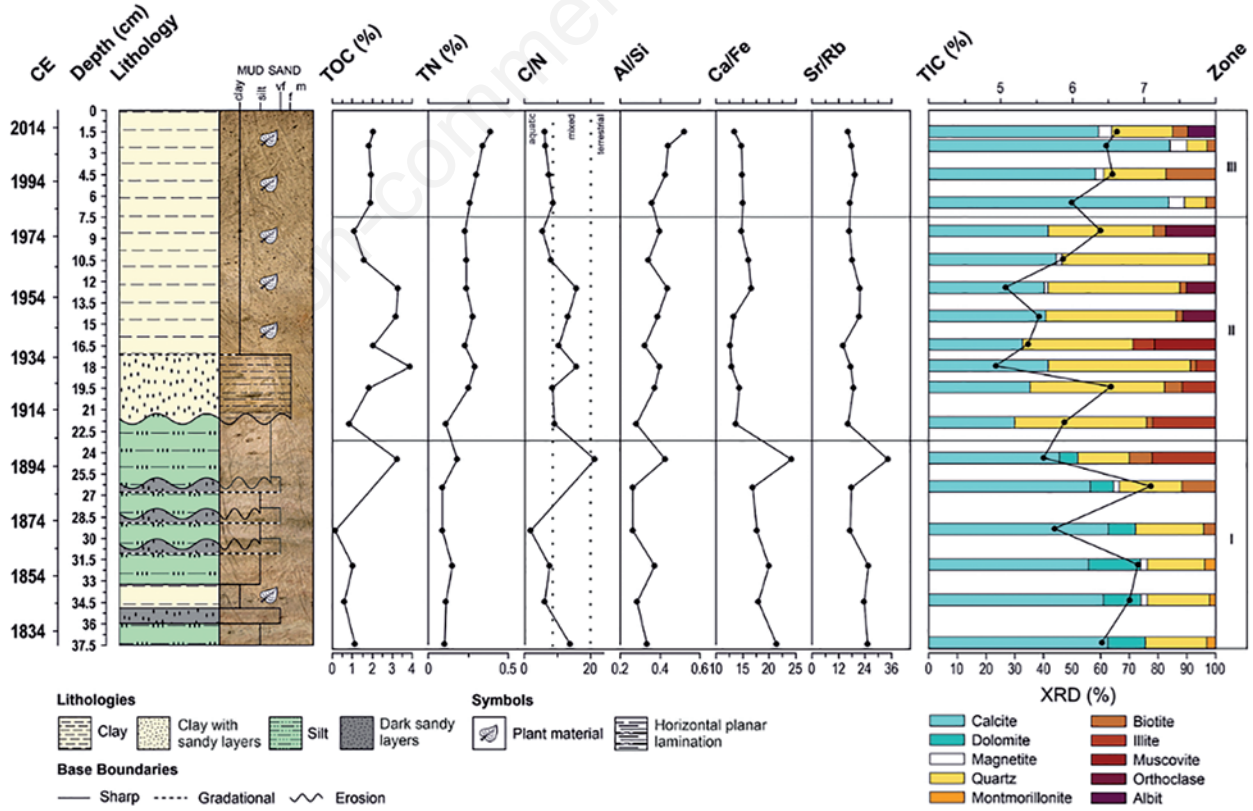

Fig. 3. Stratigraphy, environmental profiles (TOC, TIC, TN, C/N and XRF) and mineralogical profiles (XRD) of the Shen Co sediment core NC-18-40b.

TN values of the entire sediment core. C/N ratio is under 10, except at a depth of 24.5 cm, where C/N exceeds 20. Al/Si ratio ranges from 0.26-0.42. Ca/Fe ratio ranges from 14-24. Sr/Rb ratio ranges from 15.7-33.5.

Zone II (22-8.5 cm = 1909-1977 CE)

Low-Mg calcite decreases to <45 %, an opposite trend is observed for Quartz that increases up to 5 %. Illite increases to percentages of up to 22%. Muscovite shows a peak (21%) in 16.5 cm depth. Orthoclase appears with percentages of 10-17% in the upper part of this zone. Other minerals are represented with percentages of under 6% (biotite and magnetite). TOC values reach the highest values of the whole core in this zone (0.86-3.91%). TIC ranges from 5.14-6.55%. TN increases and reaches values between 0.23-0.29%. C/N ratio are higher than 10 (8-15.8). Al/Si ratio ranges from 0.3-0.4. Ca/Fe ratio decreases and ranges between 13-17. Sr/Rb ratio decreases in this zone and ranges from 134-22.

Zone III (6.5-0 cm = 1987 to the present)

The uppermost part of the core is characterized by increasing percentages of low-Mg calcite (up to 84%), a decrease in quartz (<22%). Biotite increases up to 17%. Other minerals, like magnetite and albite, are represented with low percentages (<10%). TOC values decrease and range from 1.8-2%. TIC ranges from 5.92-6.64%. TN reaches the highest values of the entire core in this zone (0.26-0.39%). C/N ratio decreases in this zone <10 (6.2-9). Al/Si ratio increases from 0.4-0.5. Ca/Fe ratio ranges between 13-15. Sr/Rb ratio ranges from 16-19.

Chironomidae assemblage

On average, 36 chironomid head capsules were counted per sample (range:0-128). A maximum number of 10 chironomid morphotypes were identified (Fig. 4, Suppl. 5 a,b), 7 are considered as non-rare taxa (relative abundance >2%) and 3 as rare taxa (abundances <2%). Regarding taxonomic identification, some head capsules could only be determined down to subfamily or tribe (*Orthocladiinae* indet. and *Tanytarsini* indet.) or genus level (*Procladius*). Three significant biostratigraphical zones were identified using Constrained Clustering (Suppl. 5c) and changes of PCA.

Zone I (37.5-19.5 cm = ~1831-1921 CE)

Zone I is characterized by a low head capsule concentration of 5.3 head capsules g^{-1} on average. The minimum number of 50 head capsules that would lead to a significant result could not be achieved. For this reason, the total number of chironomid head capsules is shown instead of percentages of abundance to avoid presenting a misleading chironomid assemblage (Fig. 3). *Procladius* is the dominant taxa reaching 14 head capsules at 20 cm depth. This chironomid also appears between 33.5-31.5 cm depth in low abundances (2-5 head capsules). *A.* indet. morphotype *incurvatus* occurs with abundances of up to 2 head capsules per sample in several samples of this zone. Other chironomid types, like *Paratanytarsus austriacus*-type and *Micropsectra radialis*-type, occurr just sporadically with abundances from 0.5-4 head capsules per sample. From 24-22 cm depth, chironomids are absent. The maximum number of morphotypes in this zone was 3, the Shannon index ranges from 0-0.9. PCA1 and PCA2 side scores were predominantly negative.

Zone II (19.5-14.5 cm = 1921-1950 CE)

Zone II is dominated by *A.* indet. morphotype *incurvatus,* reaching abundances up to 96%. *Procladius* strongly fluctuates between 0-51%, having its maximum at 17 cm. The concentration of head capsules fluctuates between 19-78 head capsules g^{-1}. Other chironomid morphotypes, such as *Paratanytarsus austriacus*-type, *Micropsectra radialis*-type, Orthocladiinae indet. and *A.* type K occur with abundances from 0 to 4%. The number of morphotypes in this zone ranges from 3 to 5, the average Shannon index is 0.55 (0-0.9). In one sample (16.5 cm), the minimum number of head capsules (50) could not be reached. PCA1 side scores are predominantly negative. PCA2 side scores are predominantly positive.

Zone III (14.5-0 cm = 1950 to the present)

Zone III is characterized by the dominance of *Procladius* (63-89%). The abundances of *A.* indet. morphotype *incurvatus* decreases from 37% at 6 cm to 6% at 2 cm, and it was no longer found from a depth of 2 cm up to the present. The shift in dominance from *A.* indet. morphotype *incurvatus* to *Procladius* is abrupt. *Psectrocladius sordidellus*-type occurs in this zone with higher abundances of up to 22% between 11-14 cm depth, and again up to 27% in the upper part of the core (0-2 cm). Other chironomid morphotypes, such as *Paratanytarsus austriacus*-type, *Micropsectra radialis*-type, Orthocladiinae indet. and *A.* type K occur with abundances of 0-4%. The concentration of head capsules fluctuates between 35-284 head capsules g^{-1} (mean 142 head capsules g^{-1}). The average number of morphotypes is 3-5, the Shannon index ranges from 0.3-0.9 (average 0.67). PCA1 side scores are predominantly positive. PCA2 side scores fluctuate around zero.

Relationship between chironomids and environmental variables

The PCA scores (Fig. 4, Suppl. 6a) explain 73% (PCA1) and 26% (PCA2) of the chironomid assemblage

variance. The gradient length of the DCA Axis 1 is 1.81 standard deviation (SD) units. This suggests that a linear method (<2 SD) such as Redundancy Analysis (RDA) is most appropriate for the ordination identifying the relations between chironomid taxa and environmental variables (Ter Braak, 1987). The RDA analysis (Fig. 5, Suppl. 6a) reveal that the first two axis explain 43% (RDA1) and 24% (RDA2) of chironomid variance, respectively. The samples belonging to Zone I are clustered in the upper right quadrant and the samples of Zone II are predominantly associated to the negative side of RDA2. Samples of Zone III are predominantly clustered in the upper left quadrant.

A. indet. morphotype *incurvatus* is distributed on the negative direction of RDA1/RDA2 and is related to the sample scores which belong to Zone II. *Procladius* and *P. sordidellus*-type are more related to Zone III. ANOVA identified TN (7.12 variance), TOC (2.76 variance), Ca/Fe (1.90 variance) and Al/Si (1.71 variance) as significant variables (Suppl. 6b). Also, Sr/Rb and C/N are other possible important variables, that were identified as non-linear non-dependent variables (VIF <20), that could explain the distribution of the chironomid types.

Lake surface area

Lake surface area (Fig. 6a, Suppl. 7) of Shen Co was 42.1 km^2 in 1973 and increased up to 44.1 km^2 in 2001.

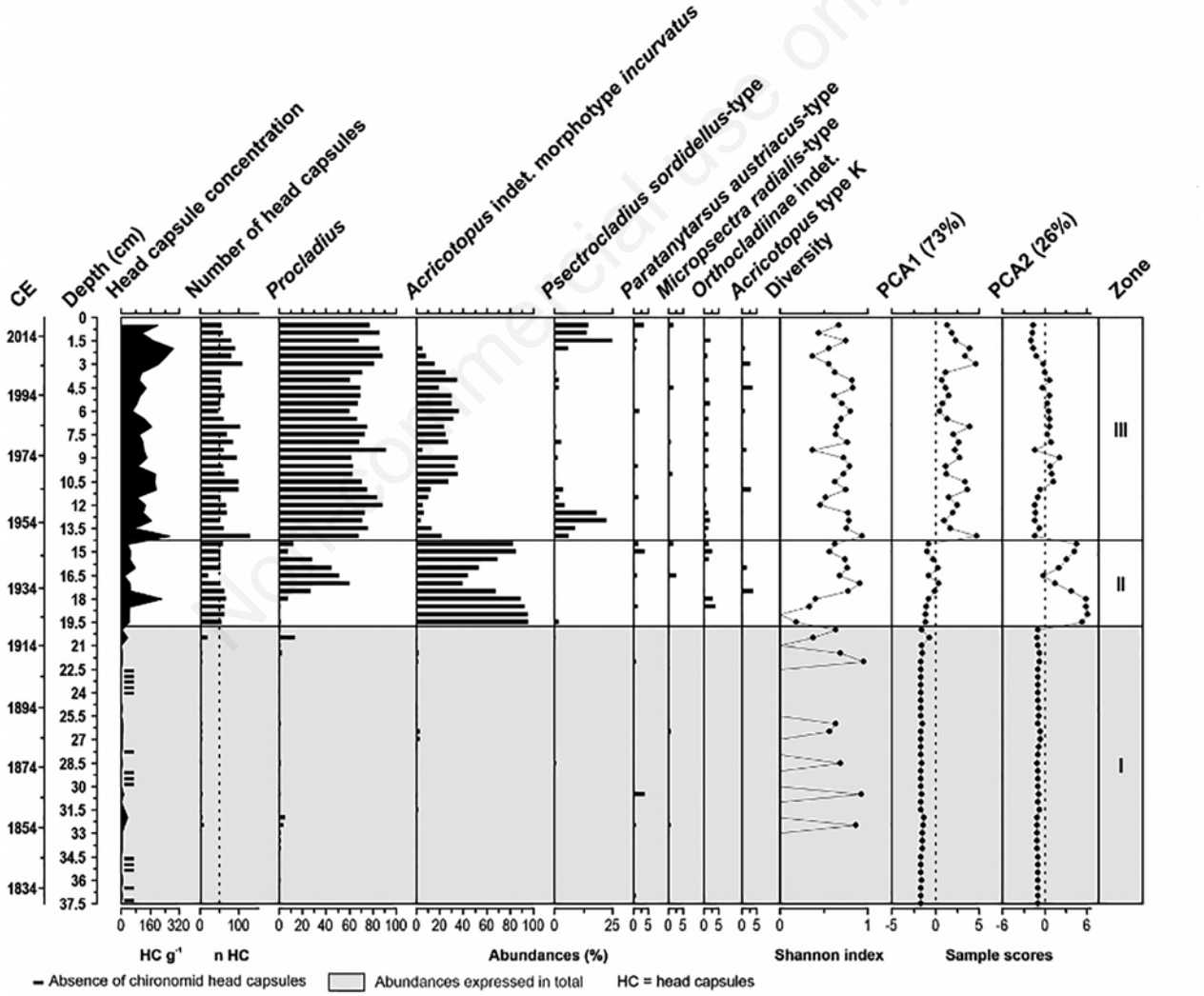

Fig. 4. Changes in chironomid assemblages in Shen Co sediment core NC-18-40b during the last ~200 years: concentration of head capsules, number of head capsules, relative abundance of principal taxa (black bars), Shannon diversity index, the first (PCA1) and second (PCA2) axis sample scores from Principal Component Analysis (PCA) of chironomid assemblage. Chironomid morphotypes are presented according to their appearance in time and abundances. Low chironomid abundances of Zone I are expressed in total abundance (grey area).

Then, a much higher and faster increase of 7 km² was detected between 2001-2008. From 2008 until today, lake surface area of Shen Co increased continuously from 51.8-52 km². From 1973-2001, an island (Fig. 6b) was visible in Shen Co. Surface area of the island decreased from 1973-2001 from 0.19-0.05 km². Nowadays (2005-2021) the island is no longer recognizable.

DISCUSSION

Low chironomid species richness and diversity in the shallow, hypersaline Shen Co during the late Holocene

Chironomidae are among the aquatic organisms with the highest tolerance to elevated salinities (Castillo *et al.*, 2018). Nevertheless, only the most specialized halophilic chironomids can survive under the extreme saline conditions (~9 g L^{-1}) of Shen Co. The low lake level (~5 m today) and the high elevation further limits the number of potential chironomids. This explains the extremely low chironomid diversity (Shannon index <1, Fig. 4) with a species richness of 7 non-rare taxa (abundance >2%) and 3 rare taxa (abundance <2%), which is low even compared to other mesohaline-haline Tibetan lakes like Selin Co (15 non-rare, 19 rare) or freshwater lakes such as Taro Co (26 non-rare, 17 rare) (Laug *et al.*, 2020a; Laug *et al.*, 2021).

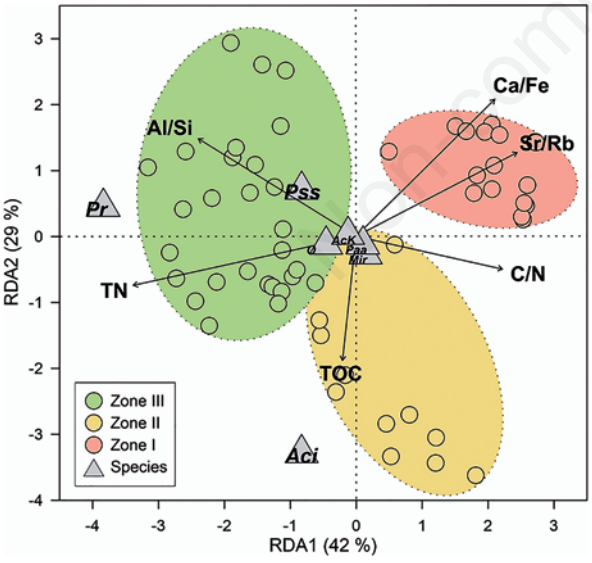

Fig. 5. Redundancy analysis plot of sample scores (circles, red=Zone I, yellow=Zone II, green=Zone III), non-rare chironomid taxa denoted with grey triangles and environmental variables (black arrows). Abbreviations of chironomid types are as follows: *AcK, Acricotopus* type K; *Aci, Acricotopus* indet. morphotype *incurvatus; Mir, Micropsectra radialis*-type; O, Orthocladiinae indet.; *Paa, Paratanytarsus austriacus*-type; *Pro, Procladius; Pss, P. sordidellus*-type.

The most common chironomid morphotypes in the Shen Co sediments, which cover the last 200 years, are *Procladius*, *A.* indet. morphotype *incurvatus* and *P. sordidellus*-type. These chironomid morphotypes have been reported as tolerant to high salinity (TDS >10,000 mg L^{-1}) and low lake levels (<8 m) (Zhang *et al.*, 2007; Chen *et al.*, 2014; Laug *et al.*, 2019). The chironomid fauna of Shen Co has similarities with those of other hypersaline, high altitude, central Tibetan lakes such as Lake Guojialin (31°59'N, 88°40'E, altitude ~4,520 m, >30.000 TDS) and Lake Nairipingcuo (31°18'N, 91°28'E, altitude 4,529 m asl, >30.000 TDS). These lakes are located at a distance of ~200 km (north-western direction) and ~100 km (north-eastern direction) to Shen Co and are also dominated by the chironomid morphotypes *Procladius* and *P. sordidellus*-type (Zhang *et al.*, 2007; Lin *et al.*, 2017).

Environmental history of Shen Co since 1831

Dry period between 1831 and 1921 CE (Zone I; 37.5-19.5 cm) – Lowest chironomid abundances

The bottom part of the core (37.5-19.5 cm) is characterized by a low number or lack of chironomid head capsules (Fig. 4). Preservation of head capsules was worse for this part of the sediment core than for the upper part. The absence of chironomids in Shen Co is mainly caused by elevated salinities, which in turn are related to low lake levels and a low inflow of fresh water, leading to a depletion of the local fauna due to osmotic stress (Williams *et al.*, 1990; Verschuren *et al.*, 2000b; Heinrichs and Walker, 2006; Laug *et al.*, 2020b). Especially in arid and semi-arid areas, salinity has a strong influence on chironomid composition in closed lakes (Verschuren *et al.*, 2000b; Brooks *et al.*, 2007; Zhang *et al.*, 2007; Chen *et al.*, 2009). Apparently, lake levels in Shen Co were so low that even our sampling site was located in the supra-littoral zone of the lake, not covered by lake water (White and Miller, 2008). The supra-littoral zone of lakes is not a suitable habitat for most of chironomid larvae even though there are a few semi-terrestrial species adapted to the highly variable environmental conditions of such habitats (Brooks *et al.*, 2007).

The hypothesis of a drier climate before 1921 is underlined both by the geochemical and the mineralogical composition found in this part of the core. In shallower lakes, mixing of the water column by winds and turbulences, and the absence of a thermocline or chemocline leads to higher oxygen saturation of the water column. This increases decomposition of TOC and indicates low lake levels (Meyers and Ishiwatari, 1993; Meyers, 2003) in the Shen Co sediments. Low values of C/N ratio in the bottom part of the core suggest a low input of terrestrial organic matter mainly due to low runoff

(Last, 2002; Meyers, 2003). In contrast to the upper part of the sediment core, the bottom part of the sedimentary sequence does not include any plant material, which suggests that there was no macrophyte vegetation in the lake at the time due to dry conditions, resulting in a low lake level and decreased terrestrial organic matter (OM) in the lake. Dry conditions are also underlined by the low Al/Si ratio, reflecting low runoff and low chemical weathering due to decreasing input into the lake by rivers or precipitation (van Hoang *et al.*, 2010; Croudace and Rothwell, 2015). Similarly, also the higher values of Ca/Fe ratio and TIC, which indicate authigenic carbonate deposition (Hou *et al.*, 2017). High Sr/Rb ratios indicate a negative precipitation/evaporation balance leading to lower lake levels and higher salinity (Zhisheng *et al.*, 2001; Li *et al.*, 2008; Kasper *et al.*, 2021) as well as a coarser grain size (Koinig *et al.*, 2003), caused by the close distance of the sampling site to the shoreline and higher terrestrial environment at the sampling site. The mineral composition of the bottom part of the core shows higher percentages of evaporite minerals such as low-Mg calcite and dolomite, which reveal a high evaporation rate during this time period. This causes evaporitic minerals to precipitate in the lake water (Oliva *et al.*, 2003; Li *et al.*, 2008). In addition, the low relative content of quartz and the simultaneously high content of low-Mg calcite and dolomite suggest low chemical weathering and low runoff (Nesbitt *et al.*, 1997; Wray and Sauro, 2017).

Periods void of chironomid head capsules in the bottom part of the core (Fig. 4, highlighted by minus signs) suggest multiple recurrent dry events at the sampling site, which occurred at 29-30 cm, 34.5-35.5 cm

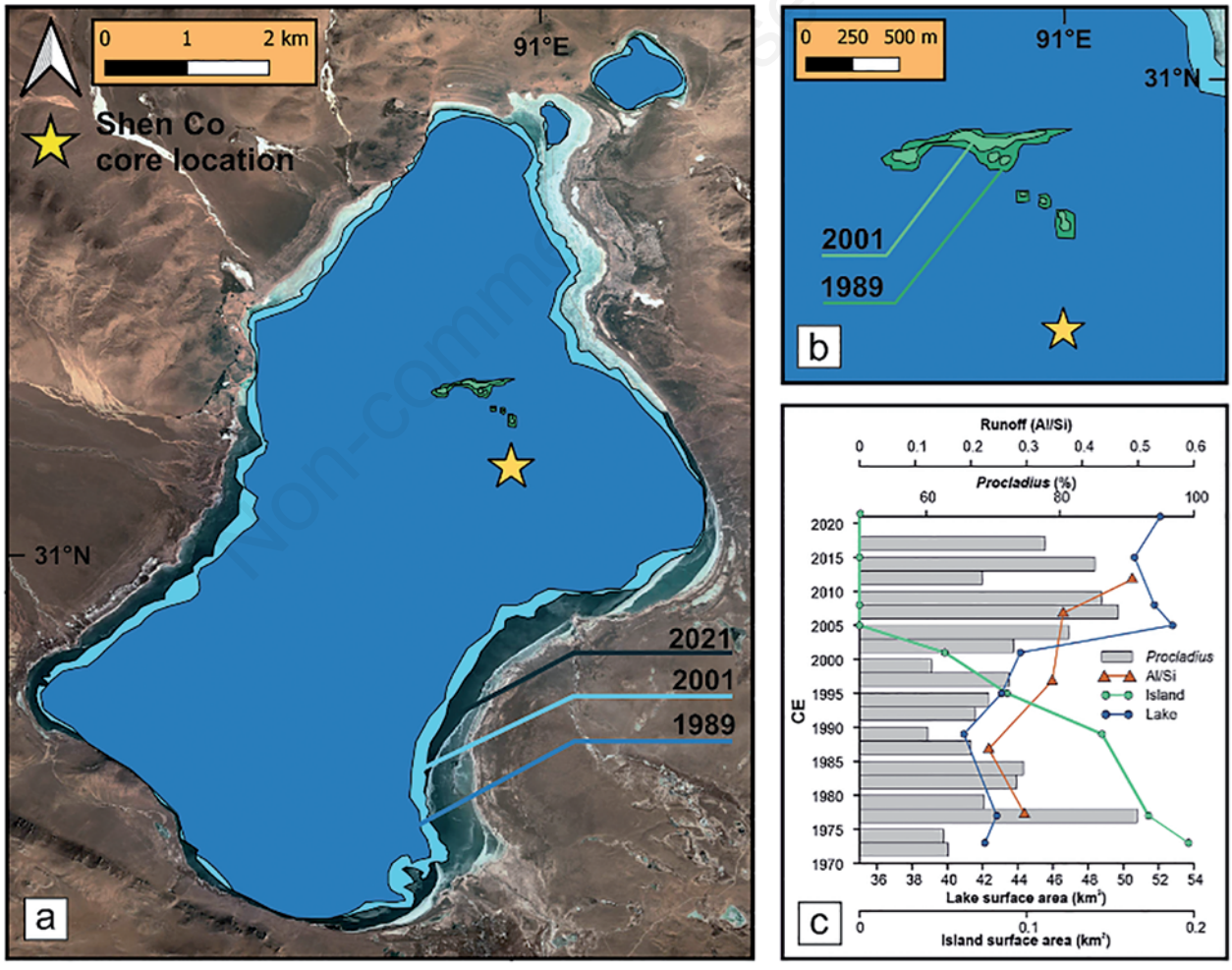

Fig. 6. a) Lake boundaries of Shen Co in 1989 (dark blue) and 2001 (light blue) taken by Landsat 4-5 and Landsat 7 ETM+ compared to present extent of Shen Co; b) former island visible in 1989 (dark green) and in 2001 (light green); c) surface area of Shen Co and island from 1973 – 2021 determined by Landsat imagery, abundance of *Procladius* (%) and Al/Si ratio as indicators of increasing lake level and runoff in Shen Co since the 1970s.

and especially at 22.5-24.5 cm, leading to a poor state of preservation of head capsules. These periods are in line with several 1 cm thick, dark, sandy layers (34-35 cm and 29-30 cm), suggesting a high-energy environment, characterized by low lake levels and high turbulences which could have resulted in a higher fragmentation of chironomid head capsules (Berntsson *et al.*, 2014; Brooks *et al.*, 2007). The dry events could have led to a more terrestrial environment and a higher input of allochthonous organic material at the coring site in relation to the autochthonous production in the lake, explaining the increase in C/N ratio to over 20. Evidence for these dry events include higher peaks of Ca/Fe, indicating high evaporation and decreasing lake levels and reflecting a negative evaporation/precipitation balance (Kasper *et al.*, 2013). The short distance of the sampling site to the shoreline led to the deposition of shoreline-facies (mainly sand) at the sampling site, resulting in a peak of the Sr/Rb ratio (Koinig *et al.*, 2003). Sedimentological data indicates that the sediments of this zone are characterized by erosive boundaries, suggesting the coring site was exposed to sub-aerial environments.

Chironomids show a slight increase in abundance mainly attributable to *Procladius*, *Paratanytarsus austriacus*-type and *A.* indet. morphotype *incurvatus,* especially between 1848 and 1866 CE and at the end of this period (~1916 CE). Time periods with higher occurrences of these chironomid types suggest brief periods of higher lake levels. The peaks of chironomid abundances in this period are accompanied by finer sediments and aquatic plant remains in contrast to the rest of the lower part of the core, which is characterized by higher proportions of sand and an absence of macrophyte remains. This suggests that within this rather arid period, there were also periods with lacustrine conditions that provided habitats for chironomids. Increasing chironomid abundances at the end of the period (22-20 cm core depth) suggest an increase in lake level and a more suitable habitat in Shen Co for chironomid larvae. This is confirmed by increasing TN and Al/Si, and decreasing Ca/Fe and Sr/Rb ratios, suggesting increasing runoff and lower evaporation, which led to higher lake levels in Shen Co.

High runoff from 1921 to 1950 CE (Zone II; 19.5-14.5 cm) – Dominance of A. indet. morphotype incurvatus

This period is characterized by increased chironomid head capsule abundances, probably a result of rising lake levels with a simultaneous decrease in salinity after 1921. Rising lake levels were probably caused by increased runoff, indicated by increasing values of the Al/Si ratio (van Hoang *et al.*, 2010; Croudace and Rothwell, 2015). Moreover, high values of TOC indicate a lower oxygen saturation at the bottom of the lake due to rising lake levels as well as an increase in terrestrial OM input suggested by moderately higher values of TN and C/N (Meyers and Ishiwatari, 1993; Meyers, 2003). Decreasing values in the Sr/Rb and Ca/Fe ratios indicate an increase in weathering (Zhisheng *et al.*, 2001; Li *et al.*, 2008; Croudace and Rothwell, 2015; Kasper *et al.*, 2021), as well as stronger precipitation and lower salinities after 1921.

Chironomid assemblages are dominated by high abundances of *A.* indet. morphotype *incurvatus,* which is found in high-elevation lakes and ponds and has so far only been described from lakes on the Tibetan Plateau. The larvae occur in fresh to saline water bodies (~0.5-35 m water depth), prefer sandy substrates and are not associated with macrophyte vegetation (Hamerlík *et al.*, 2010; Laug *et al.*, 2018; Laug *et al.*, 2019; Laug *et al.*, 2020a). Although no ecological studies of this morphotype have been conducted, it seems that the larvae of *A.* indet. morphotype *incurvatus* live and feed on the sediment of lakes, proved by finding of sediment in the gastrointestinal tract of larvae from *A.* indet. morphotype *incurvatus* (Laug *et al.*, 2019).

The dominance of *A.* indet. morphotype *incurvatus* in the transition zone from low to higher lake levels might be explained by a phase of turbid, sandy water void of submerged macrophytes (Laug *et al.*, 2019; Laug *et al.*, 2020a), a likely state during the pioneer phase of the lake (Laug *et al.*, 2019; Laug *et al.*, 2020a). By preferring sandy sediments and habitats without macrophytes, *A.* indet. morphotype *incurvatus* is an excellently adapted pioneer in the forming lake. The dominance of this morphotype allows two conclusions to be drawn for Shen Co:i) the lake level had risen enough (>0.5 m) so that the core location was no longer in the supralittoral zone, and ii) the macrophyte vegetation had not yet been established. For this reason, the macrophyte-associated morphotypes such as the *Paratanytarsus austriacus*-type and *P. sordidellus*-type are absent.

The dominance of sandy substrate during this period, which is favored by increased fluvial transport and increasing runoff (Dypvik and Harris, 2001; Kylander *et al.*, 2013), also underlines the hypothesis of higher runoff and lake levels at the sampling site. Sedimentological analysis revealed fine laminations during this period, which could have been a result of higher water levels. Laminations, which are characterized by small differences in grain size, are indicators of variations in input, chemical conditions or biological activity and represent changes in sedimentary input (Kemp, 1996). The dominance of quartz in the sediment, accompanied by an absence of unstable minerals such as dolomite and montmorillonite, may indicate strong weathering processes due to wet conditions characterized by high runoff in fluvial systems (Nesbitt *et al.*, 1997). The stratigraphy also shows a gradual superior contact into the next period that suggests a continuous increase in lake level.

Lake level rise after 1950 CE (Zone III; 14.5-0 cm) – Dominance of Procladius and P. sordidellus-type

The most recent period is dominated by *Procladius* and *P. sordidellus*-type, replacing *A.* indet. morphotype *incurvatus.* As a free-swimming predator, *Procladius* occurs in lakes deeper than 2 m (Erbaeva and Safronova, 2016). In addition, some studies associate *Procladius* with soil erosion (Zhang *et al.*, 2013; Chang *et al.*, 2018) and finer sediment (Hamerlík *et al.*, 2010). For this reason, we attribute the presence of *Procladius* in Shen Co to higher lake levels, with water depths above 2 m, and clayey substrate. The lower Sr/Rb ratio in this part of the core indicates a finer grain size, which is likely due to an increase in the distance from the shoreline to the sampling site and less coarse terrestrial material being introduced as a result of the higher lake level. The absence of clay minerals in the upper part of the core also supports the notion of a warmer and wetter climate in the Shen Co catchment with higher precipitation and runoff into the lake (Nesbitt *et al.*, 1997).

Procladius reaches its highest abundances in the uppermost two centimeters of the sediment core. Therefore, the highest lake levels of the record are proposed to have occurred since 2006 CE. This is supported by high TN values and high Al/Si ratios and is in line with the Landsat imageries from Shen Co during 1973-2021, which document a strong rise in lake levels between 2001 and 2005 CE (Fig. 6c). The extreme, abrupt shifts from *A.* indet. morphotype *incurvatus* to *Procladius* and *P. sordidellus*-type can be explained as follows. The larvae of the later instars of *Procladius* are the top predators in the food chain, feeding on Crustacea, other chironomid larvae and Oligochaeta (Baker and McLachlan, 1997; Brooks *et al.*, 2007). Field experiments have demonstrated that *Procladius* exerts hunting pressure on other chironomid types (*e.g.*, *Chironomus*) and that prey density decreases on predation by *Procladius* (Hershey, 1986). For this reason, the decreasing abundances of *A.* indet. morphotype *incurvatus* could be explained by the occurrence of *Procladius* and the resulting hunting pressure on that morphotype, especially during periods when other food sources were not available due to the relatively extreme habitat, characterized by high salinity and low macrophyte vegetation. The other, possibly more likely explanation would be that increased lake levels increased the number of potential habitats and made the habitat unsuitable for the detritus-feeding *A.* indet morphotype *incurvatus*.

Some studies report that periods of high submerged aquatic plant cover are characterized by correspondingly high abundances of macrophyte-associated chironomid species in lake sediments (Mason and Bryant, 1974; Ramcharan and Paterson, 1978; Brodin, 1986; Brodersen *et al.*, 2001). *P. sordidellus*-type is often described as a littoral, phytophilic taxa, which is associated with aquatic macrophytes (Brodersen *et al.*, 2001; Brooks *et al.*, 2007; Moller Pillot, 2013; Nazarova *et al.*, 2017; Laug *et al.*, 2019). Higher abundances of *P. sordidellus*-type in the upper part of the sediment core are probably triggered by the occurrence of aquatic macrophyte vegetation. Low abundances of *A.* indet. morphotype *incurvatus* during both *P. sordidellus*-type maxima, a morphotype which apparently needs macrophyte-free sandy substrate (Laug *et al.*, 2019), supports this assumption.

A decline in macrophytes could have been triggered by higher turbidity caused by higher precipitation and sediment fluxes into the lake, which leads to reduced light intensity in the bottom sediments (Laug *et al.*, 2020a). Other reasons could have been mechanical damage of the macrophytes by wind (Phan-Garrigues *et al.*, 2020) and ice-covering of shallow lakes that can reduce macrophyte growth (Morrill *et al.*, 2006). The growth of macrophytes is thus inhibited during the period characterized by very low lake levels (1831-1950 CE) and strong inflow (~1910-1920 CE), and macrophyte-related taxa such as *P. sordidellus*-type do not occur. Macrophyte vegetation increased with higher lake levels after 1950 CE, which inhibited mechanical damage by wind and increased transparency due to a weaker inflow. Such abrupt changes in macrophyte vegetation are caused primarily by external influences. Increased water and sediment input may lead to increased turbidity in the water body, which is followed by a decline in submerged macrophyte vegetation. This may have led to a tipping point, causing a complete collapse of macrophyte vegetation. Recovery of the system and recolonization by macrophytes may have been brought about by a reduction in precipitation and sediment inputs (Laug *et al.*, 2020a). The rise in lake level after 1950 CE probably had the effect of weakening wind-induced turbulence at the lake bottom and, in combination with lower salinity and the higher input of organic material, improved the habitat for aquatic macrophytes. The C/N ratio decreases in this part of the core (<10), suggesting a predominance of autochthonous productivity, which indicates decreasing terrestrial input and rising lake levels at the sampling site (Last, 2002). This observation supports the theory of a change from a turbid, macrophyte-free state to a macrophyte-covered, clear lake (Laug *et al.*, 2020b). Furthermore, the influence of algae and aquatic macrophytes is higher in Zone III compared to the previous zones. The highest TN values were observed in the youngest part of the sediment core, suggesting increasing nutrient availability in Shen Co in recent decades, which in turn may have been a result of developing macrophyte vegetation in the lake. The low abundances of *P. sordidellus*-type between 1967 and 2007 CE is probably explained by low macrophyte cover. At this time abundances of *A*. indet. morphotype *incurvatus* also increased.

Potential forcing mechanisms

The Shen Co chironomid record spans the last two centuries and represents the end of the Little Ice Age (up until 1850 CE) and the Current Warm Period (since 1850 CE to present). According to the chironomid stratigraphy, geochemical, sedimentological and mineralogical analyses, the catchment of Shen Co experienced two distinct periods of moisture development:a relatively dry period lasting from 1831 to 1921 CE and a subsequent wetter period from 1921 CE until today.

The most recent meteorological station data on the Tibetan Plateau (Li *et al.*, 2010; Yang *et al.*, 2011; Lei *et al.*, 2014a; Yang *et al.*, 2014a) as well as climate models (Su *et al.*, 2013) show that precipitation has increased here during the last 40 years (Ma *et al.*, 2018; Sun *et al.*, 2020) and that the Tibetan Plateau has experienced a trend toward wetter conditions in this time period (Yang *et al.*, 2003; Chen *et al.*, 2013; Wang *et al.*, 2018; Sun *et al.*, 2020). The central Tibetan Plateau, especially the Naqu region, in which both Nam Co and Shen Co are located, was affected by increasing annual precipitation of 15 mm per decade (Fang *et al.*, 2016) from 1970 to 2010 CE. As a result of this increase in precipitation, lake levels in the majority of lakes on the northern and central Tibetan Plateau, including Shen Co (Fig. 6), are rising (Morrill, 2004; Lei *et al.*, 2013; Gao *et al.*, 2014; Lei *et al.*, 2014a, 2014b; Wan *et al.*, 2014; Fang *et al.*, 2016; Ma *et al.*, 2016; Jiang *et al.*, 2017; Yang *et al.*, 2017; Zhang *et al.*, 2021). In contrast, the levels of lakes on the southern Tibetan Plateau have decreased due to low precipitation as well as decreasing meltwater input from glaciers and permafrost (Gao *et al.*, 2014; Lei *et al.*, 2014a; Fang *et al.*, 2016; Zhang *et al.*, 2021). The rise in lake levels is further exacerbated by declining potential evaporation rates (~13 mm per decade) on the central Tibetan Plateau between 1979 and 2016 CE (Fang *et al.* 2016), due to lower wind speeds and lower solar radiation (Lei *et al.*, 2014a; Yang *et al.*, 2014a).

The chironomid record from Shen Co is in line with other records (Suppl. 8) that support an increase in precipitation on the northern and central Tibetan Plateau during the Current Warm Period. The Dunde (38°13'N; 96°63'E; 5,325 m a.s.l.) and Guliya (35°17'N, 81°29'E) ice caps are situated on the northern part of the Tibetan Plateau. Ice core records (Fig. 7) from these sites show an enrichment of oxygen isotope ($\delta^{18}O$) values in the 20th century due to increasing temperatures and higher snow accumulation rates (Thompson *et al.*, 1989; Thompson *et al.*, 1997; Yao *et al.*, 1997), indicating higher precipitation since the beginning of the last century. The same patterns were determined in $\delta^{18}O$ values of an ice core from the Puruogangri ice cap (33°55'N, 89°05'E; 6,072 m asl), showing an increase in temperatures between 1910 and 1920 CE (Fig. 7) (Thompson *et al.*, 2006). This suggests a shift to a warmer, wetter climate since 1920 CE on the central Tibetan Plateau (Thompson *et al.*, 2006). Salinity reconstructions (Sal_{ch}) based on a chironomid record from Lake Sugan reveal a decrease in effective moisture between the mid-18th century and the beginning of the 19th century. Slightly rising moisture is represented by higher abundances of low-saline-water chironomid taxa (Chen *et al.*, 2009) since the 1920s. Mean annual precipitation (MAP) reconstructions (Fig. 7) from the central Tibetan Plateau based on tree-rings (Yang *et al.*, 2014b) and pollen assemblages (Cui *et al.*, 2021) suggest a rise in precipitation in regions that are influenced by both Westerlies and the EASM during the last century. This is also underlined by records from the eastern Tibetan Plateau, which are dominated by the EASM. Sedimentary records from Lake Nir'pa Co (Bird *et al.*, 2017) and Lake Ximencuo support a shift to wetter conditions during the 20th century, indicated by a rise of silt content as a consequence of increased erosion (Bird *et al.*, 2017), as well as rising TOC and TN (Pu *et al.*, 2013). This suggests higher fluvial input as a result of enhanced precipitation in the catchment area. MAP reconstructions from Lake Kusai highlight a dry phase until 1900 CE and a precipitation maximum in 1920 CE and 1950 CE, corresponding to chironomid assemblage shifts in 1920 and 1950 from Shen Co. In contrast, climate records from the southern margin of the Tibetan Plateau, which are dominated by the ISM, show different results to those of the chironomid record from Shen Co, like decreasing precipitation and dryer conditions.

There are several explanations for these different precipitation patterns on the Tibetan Plateau, which mainly focus on changes of the Asian monsoonal system (Chen *et al.*, 2021). Many studies have suggested that the ISM has weakened since the mid-20th century, as reflected in declining rainfall on the southern Tibetan Plateau and in the Himalayas (Duan *et al.*, 2006; Lei *et al.*, 2014a, 2014b; Sheng *et al.*, 2015; Dutt *et al.*, 2018; Thompson *et al.*, 2018). The weakening of the ISM may have primarily been a result of warming and reduced wind strength in the region, which have resulted in weakened water vapor exchange between the Indian sub-continent and the Tibetan Plateau, leading to a decrease in precipitation on the southern Tibetan Plateau (Yang *et al.*, 2014a; Sheng *et al.*, 2015). The EASM index of IPCC shows a strengthening of the EASM at the beginning of the 20th century (around 1910 CE) and a weakening trend in the second half of the last century (IPCC, 2007, 2021).

The enhanced increase in precipitation on the inner Tibetan Plateau since the end of the 20th century is attributed to altered anticyclone and cyclone areas over the eastern and western Tibetan Plateau, respectively. These weaken the westerlies and thus retain water vapor over the Tibetan Plateau and facilitate water vapor intrusion from the south (Sun *et al.*, 2020). Crucial to these atmospheric changes on the Tibetan Plateau is the

Atlantic multidecadal oscillation (AMO), which has been in a warm phase since the mid-1990s and is responsible for the cyclonic and anticyclonic variances on the Tibetan Plateau (Sun *et al.*, 2020). An overall wetting trend of the arid regions of central Asia after 1958 CE was considered to have resulted from a weakening EASM, which led to reinforced monsoonal water vapor transport towards the arid, northern regions of the Tibetan Plateau (Chen *et al.*, 2021). Most of these studies demonstrate an increasing influence of the EASM on the arid areas of the Tibetan Plateau. Stalagmite records from Wanxiang cave and Dongge cave (Central China) also indicate a weakening trend of the EASM for the time period 1960 – 2000 CE (Yuan *et al.*, 2004; Zhang *et al.*, 2008b). Westerly winds also appear to be subject to a weakening trend, as reflected by a positive winter Northern Atlantic Oscillation (NAO) / negative summer NAO since 1970 CE (Cornes *et al.*, 2013; Wirth *et al.*, 2013). Nevertheless, the westerly winds and monsoon systems are subject to multidecadal cycles of ~200 years (Westerlies), ~88 and ~60 years (ASM), with alternating weaker and stronger activities (Cui *et al.*, 2021). Peaks of high precipitation anomalies on the inner Tibetan Plateau in 1920 CE and 1950 CE are attributed to overlapping cycles of the Westerlies and the monsoonal systems (Cui *et al.*, 2021). These anomalies match well with the Shen Co chironomid record, showing chironomid assemblage shifts related to precipitation changes around 1920 CE and 1950 CE.

Even though knowledge of regional precipitation patterns and atmospheric circulation on the Tibetan Plateau has increased, the effects of global climate warming, aerosols, land surface conditions and global climate triggers such as the El Niño–Southern Oscillation, Indian Ocean Dipole or NAO on the precipitation patterns

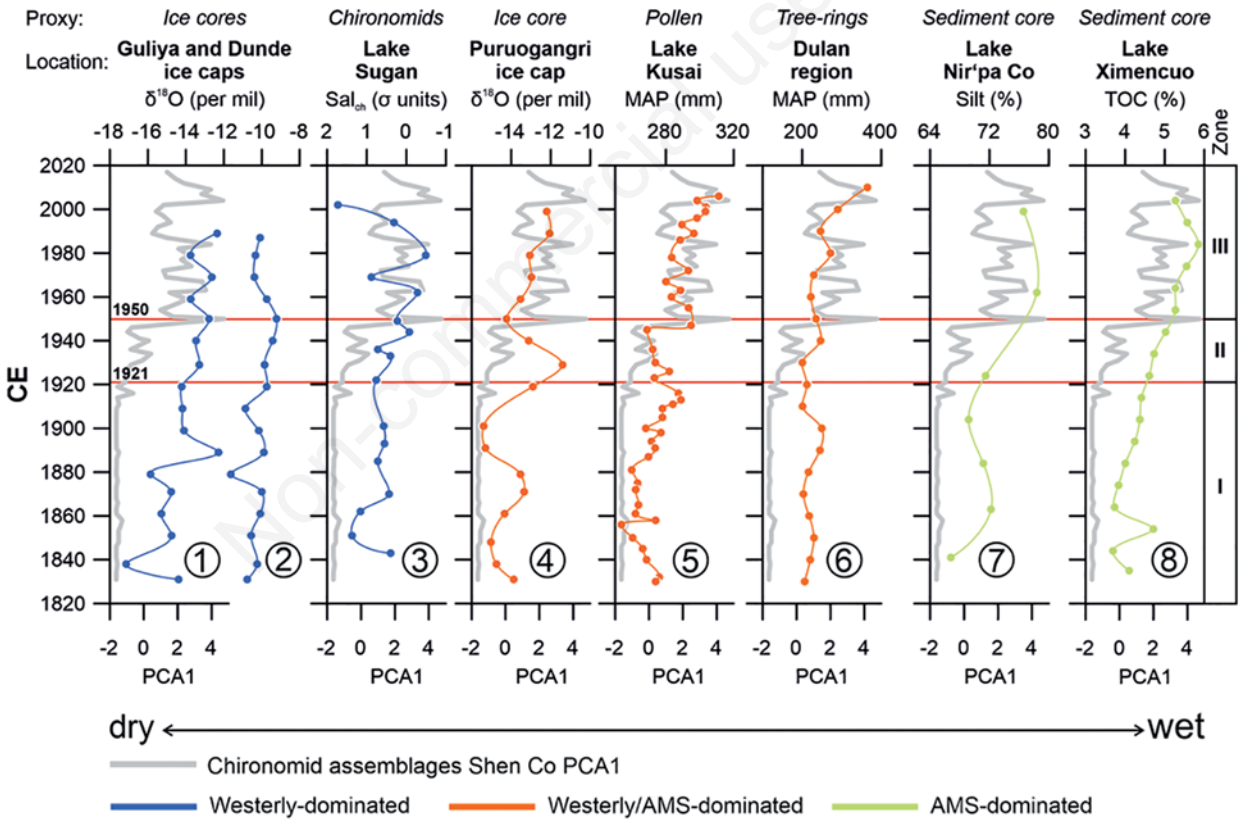

Fig. 7. Comparison of PCA1 of chironomid analysis (grey line) from Shen Co with spline-smoothed climate records from the Tibetan Plateau, showing an increase of temperatures and precipitation during the 20th century:(1) $\delta^{18}O$ ice core from Guliya ice cap (Thompson *et al.*, 1989), (2) $\delta^{18}O$ ice core from Dunde ice cap (Thompson *et al.*, 1997), (3) Chironomid salinity reconstruction from Lake Sugan (Chen *et al.*, 2009), (4) $\delta^{18}O$ ice core from Puruogangri ice cap (Thompson *et al.*, 2006), (5) Mean annual precipitation (MAP) reconstructed from pollen from Lake Kusai (Cui *et al.*, 2021), (6) Tree ring precipitation reconstruction from Dulan (Yang *et al.*, 2014b), (7) Silt amount of lake sediments from Lake Nir'pa Co (Bird *et al.*, 2017) and (8) TOC content from lake sediments from Lake Ximencuo (Pu *et al.*, 2013). Dotted, horizontal lines indicate chironomid species shifts of Shen Co around 1920 and 1950 CE. All plots were fitted using spline smoothing (Suppl. 8). Locations of records are presented in Fig. 1. Ice core, tree ring, pollen, chironomid, and lake sediment datasets were downloaded from the website of the National Oceanic and Atmospheric Administration (https://www.ncdc.noaa.gov/cdo-web/).

of the Tibetan Plateau are complex and not yet fully understood (Liu *et al.*, 2016). Due to increasing surface temperatures on the Tibetan Plateau (1.8-4.7°C projected for the 21st century (Su *et al.*, 2013)), which will intensify monsoonal precipitation in the future (Xu *et al.*, 2008; Wang *et al.*, 2018), it is projected that precipitation could increase by 6-12% between 2036 CE and 2099 CE (Su *et al.*, 2013). Atmospheric circulation models also forecast an increase in East Asian precipitation due to rising temperatures on the Tibetan Plateau (Wang *et al.*, 2008). Intensified precipitation could lead to increased surface runoff, rising lake levels (You *et al.*, 2008; Zhang *et al.*, 2017d) and the enhanced transport of material into the lake due to higher fluvial transport (Schütt *et al.*, 2010) into the Tibetan lakes, resulting in changes in the lakes' chemical composition. This will affect both water quality for a large part of the Asian population and habitat conditions for the living aquatic communities in the lakes.

CONCLUSIONS

A high-resolution combined chironomid, mineralogical and geochemical record was developed for Shen Co, Tibetan Plateau, in order to reconstruct hydrological changes, such as lake level changes, precipitation changes, runoff and changes in macrophyte vegetation in a high-altitude, shallow lake system. Prior to 1921, Shen Co had the lowest abundances of chironomid larvae due to high salinity, likely caused by high evaporation and low water input. A possible drying event could be identified for the time period 1889-1909 CE. Evidence for a drier period include a high amount of evaporite minerals, like low-Mg calcite and dolomite, as well as high Ca/Fe and Sr/Rb ratios. Lower evaporation and higher precipitation and inflow, indicated by rising TOC, TN and Al/Si ratios as well as higher amounts of quartz, caused the lake level to rise and led to a higher abundance of chironomids after 1921 CE. *A.* indet. morphotype *incurvatus, Procladius* and *P. sordidellus*-type proved to be excellent indicators of lower and higher lake levels, respectively. *A.* indet. morphotype *incurvatus* represents a period with rising lake levels until 1950 CE and appears to be a good colonizer species, attributed to high runoff. *Procladius* indicates high lake level periods since 1950 CE, with a more pronounced increase in lake levels since 2006 as a result of increasing precipitation and decreased evaporation on the central Tibetan Plateau. *P. sordidellus*-type was sensitive to the variability of macrophyte vegetation in the from 1955 to 1960 and 2011 to 2018 CE. Climate records from the northern and central Tibetan Plateau indicate that increasing precipitation on the central Tibetan Plateau since the beginning of the 20th century has led to the formation of the current lake. Due to the overlapping cycles of atmospheric currents such as the Westerlies and the Asian monsoons, 1921 and 1950 appear to have been years with increased precipitation.

ACKNOWLEDGEMENTS

We thank all the colleagues from Nam Co Observation and Research Station (NAMORS) for their help during fieldwork in Nam Co region. This research is a contribution to the International Research Training Group "Geo-ecosystems in transition on the Tibetan Plateau (TransTiP)", funded by Deutsche Forschungsgemeinschaft (DFG grant 317513741 / GRK 2309). We acknowledge support by the German Research Foundation and the Open Access Publication Funds of the Technische Universität Braunschweig.

CONTRIBUTIONS

PGEG, LP, JM, designed the study; WK, NB, AS, PP, performed sampling and limnological measurements; SR, AL, conducted Chironomidae analysis; BW, constructed the age model; PH, provided sediment-geochemical analyses and interpretation; RMA, PGEG, SR, performed sedimentological analysis and interpretation; PGEG, RMA, AL, AS, JM, LP, JW, NB, LZ, PH, A Schwalb revised and helped improve the manuscript; A Schwalb, developed the program (DFG GRK 2309/1) that funded this research; SR, wrote the manuscript with contributions from all authors. All the authors read and approved the final version of the manuscript and agreed to be accountable for all aspects of the work.

CONFLICT OF INTEREST

The authors declare that they have no competing interests, and all authors confirm accuracy.

REFERENCES

Anderson MJ, Ellingsen KE, McArdle BH, 2006. Multivariate dispersion as a measure of beta diversity. Ecol. Lett. 9:683-693.

Anslan S, Azizi Rad M, Buckel J, Echeverria Galindo P, Kai J, Kang W, Keys L, Maurischat P, Nieberding F, Reinosch E, Tang H, Tran TV, Wang Y, Schwalb A, 2020. Reviews and syntheses: How do abiotic and biotic processes respond to climatic variations at the Nam Co catchment (Tibetan Plateau)? Biogeosciences 17:1261-1279.

Appleby PG, Nolan PJ, Gifford DW, Godfrey MJ, Oldfield F, Anderson NJ, Battarbee RW, 1986. 210Pb dating by low background gamma counting. Hydrobiologia 141:21-27.

Appleby PG, Richardson N, Nolan PJ, 1992. Self-absorption corrections km well-type germanium detectors. Nucl. Inst. Methods B 71:228-233.

Baker AS, McLachlan AJ, 1997. Food preferences of

tanypodinae larvae (Diptera: Chironomidae). Hydrobiologia 62:283-288.

Bennett KD, 1996. Determination of the number of zones in a biostratigraphical sequence. New Phytol. 132:155-170.

Berntsson A, Rosqvist GC, Velle G, 2014. Late-Holocene temperature and precipitation changes in Vindelfjällen, mid-western Swedish Lapland, inferred from chironomid and geochemical data. Holocene 24:78-92.

Bitušík P, Hamerlík, L, 2014. Príručka na určovanie lariev pakomárov (Diptera: Chironomidae) Slovenska Časť 2. Tanypodinae. [Identification guide of Slovakian chironomid larvae (Diptera: Chironomidae). Part II. Tanypodinae]. [Book in Slovak]. Belianum. Matej Bel University Publ., Banská Bystrica. p. 96.

Bird BW, Lei Y, Perello M, Polissar PJ, Yao T, Finney B, Bain D, Pompeani D, Thompson LG, 2017. Late-Holocene Indian summer monsoon variability revealed from a 3300-year-long lake sediment record from Nir'pa Co, southeastern Tibet. Holocene 27:541-552.

Bolch T, Yao T, Kang S, Buchroithner MF, Scherer D, Maussion F, Huintjes E, Schneider C, 2010. A glacier inventory for the western Nyainqentanglha Range and the Nam Co Basin, Tibet, and glacier changes 1976–2009. Cryosphere 4:419-433.

Bowman JS, Sachs JP, 2008. Chemical and physical properties of some saline lakes in Alberta and Saskatchewan. Saline systems 4:3.

Brodersen KP, Odgaard BV, Vestergaard O, Anderson NJ, 2001. Chironomid stratigraphy in the shallow and eutrophic Lake Søbygaard, Denmark: chironomid–macrophyte co-occurrence. Freshwater Biol. 46:253-267.

Brodin YW, 1986. The Postglacial History of Lake Flarken, Southern Sweden, Interpreted from Subfossil Insect Remains. Int. Rev. ges. Hydrobiol. 71:371-432.

Brooks SJ, 2006. Fossil midges (Diptera: Chironomidae) as palaeoclimatic indicators for the Eurasian region. Quat. Sci. Rev. 25:1894-1910.

Brooks SJ, Langdon PG, Heiri O, 2007. The identification and use of Palearctic Chironomidae larvae in palaeoecology. QRA Technical Guide No. 10. Quaternary Research Association, London: 275 pp.

Cai Y, Ke C-Q, Li X, Zhang G, Duan Z, Lee H, 2019. Variations of Lake Ice Phenology on the Tibetan Plateau From 2001 to 2017 Based on MODIS Data. J. Geophys. Res. Atmos. 124:825-843.

Castillo AM, Sharpe DMT, Ghalambor CK, León LF de, 2018. Exploring the effects of salinization on trophic diversity in freshwater ecosystems: a quantitative review. Hydrobiologia 807:1-17.

Chang JC, Zhang E, Liu E, Shulmeister J, 2017. Summer temperature variability inferred from subfossil chironomid assemblages from the south-east margin of the Qinghai–Tibetan Plateau for the last 5000 years. Holocene 27:1876-1884.

Chang JC, Shulmeister J, Gröcke DR, Woodward CA, 2018. Toward more accurate temperature reconstructions based on oxygen isotopes of subfossil chironomid head-capsules in Australia. Limnol. Oceanogr. 63:295-307.

Chen J, Chen F, Zhang E, Brooks SJ, Zhou A, Zhang J, 2009. A 1000-year chironomid-based salinity reconstruction from varved sediments of Sugan Lake, Qaidam Basin, arid Northwest China, and its palaeoclimatic significance. Chin. Sci. Bull. 54:3749-3759.

Chen H, Zhu Q, Peng C, Wu N, Wang Y, Fang X, Gao Y, Zhu D, Yang G, Tian J, Kang X, Piao S, Ouyang H, Xiang W, Luo Z, Jiang H, Song X, Zhang Y, Yu G, Zhao X, Gong P, Yao T, Wu J, 2013. The impacts of climate change and human activities on biogeochemical cycles on the Qinghai-Tibetan Plateau. Global Change Biol. 19:2940-2955.

Chen J, Zhang E, Brooks SJ, Huang X, Wang H, Liu J, Chen F, 2014. Relationships between chironomids and water depth in Bosten Lake, Xinjiang, northwest China. J. Paleolimnol. 51:313-323.

Chen D, Zhang X, Xu B, Zhang Y, Fan J, Yao T, Guo Z, Hou Z, Cui P, Zhang T, 2015. Assessment of past, present and future environmental changes on the Tibetan Plateau. Chin. Sci. Bull. 60:3025-3035.

Chen C, Zhang X, Lu H, Jin L, Du Y, Chen F, 2021. Increasing summer precipitation in arid Central Asia linked to the weakening of the East Asian summer monsoon in the recent decades. Int. J. Climatol. 41:1024-1038.

Cornes RC, Jones PD, Briffa KR, Osborn TJ, 2013. Estimates of the North Atlantic Oscillation back to 1692 using a Paris-London westerly index. Int. J. Climatol. 33:228-248.

Croudace IW, Rothwell RG, 2015. Micro-XRF Studies of sediment cores. Springer, Dordrecht: 668 pp.

Cui A, Lu H, Liu X, Shen C, Xu D, Xu B, Wu N, 2021. Tibetan Plateau precipitation modulated by the periodically coupled Westerlies and Asian Monsoon. Geophys. Res. Lett. 48:e2020GL091543.

Dong S, Peng F, You Q, Guo J, Xue X, 2018. Lake dynamics and its relationship to climate change on the Tibetan Plateau over the last four decades. Reg. Environ. Change 18:477-487.

Downs RT, Hall-Wallace M, 2003. The American Mineralogist crystal structure database. Am. Mineral. 88:247-250.

Dr. H. Putz & Dr. K. Brandenburg GbR. Match! Crystal Impact, Kreuzherrenstr. 102, 53227 Bonn, Germany.

Duan K, Yao T, Thompson LG, 2006. Response of monsoon precipitation in the Himalayas to global warming. J. Geophys. Res. 111:D19110.

Dutt S, Gupta AK, Wünnemann B, Yan D, 2018. A long arid interlude in the Indian summer monsoon during ~4,350 to 3,450 cal. yr BP contemporaneous to displacement of the Indus valley civilization. Quat. Int. 482:83-92.

Dypvik H, Harris NB, 2001. Geochemical facies analysis of fine-grained siliciclastics using Th/U, Zr/Rb and (Zr+Rb)/Sr ratios. Chem. Geol. 181:131-146.

Eggermont H, Heiri O, Verschuren D, 2006. Fossil Chironomidae (Insecta: Diptera) as quantitative indicators of past salinity in African lakes. Quat. Sci. Rev. 25:1966-1994.

Erbaeva EA, Safronova GP, 2016. Register of Chironomids (Diptera, Chironomidae) of the Lake Khubsugul in Mongolia, p. 221–244. In: A. Stubbe (ed.), Erforschung biologischer Ressourcen der Mongolei. Martin-Luther-Universität Halle-Wittenberg.

Fang Y, Cheng W, Zhang Y, Wang N, Zhao S, Zhou C, Chen X, Bao A, 2016. Changes in inland lakes on the Tibetan Plateau over the past 40 years. J. Geogr. Sci. 26:415-438.

Ferrington LC, 2008. Global diversity of non-biting midges

(Chironomidae; Insecta-Diptera) in freshwater. Hydrobiologia 595:447-455.

Gao Y, Cuo L, Zhang Y, 2014. Changes in Moisture Flux over the Tibetan Plateau during 1979–2011 and Possible Mechanisms. J. Climate 27:1876-1893.

Greffard M-H, Saulnier-Talbot É, Gregory-Eaves I, 2012. Sub-fossil chironomids are significant indicators of turbidity in shallow lakes of northeastern USA. J. Paleolimnol. 47: 561-581.

Grimm EC, 1987. CONISS: A Fortran 11 program for stratigraphically constrained cluster analysis by the method of incremental cluster analysis by the method of incremental sum of squares. Comput. Geosci. 13:13-35.

Hamerlík L, Christoffersen KS, Brodersen KP, 2010. Short comment on chironomid assemblages and stratigraphy of high altitude lakes from Tibet. J. Chiron. Res. 23661.

Heinrichs ML, Walker IR, Mathewes RW, 2001. Chironomid-based paleosalinity records in southern British Columbia, Canada: a comparison of transfer functions. J. Paleolimnol. 26:147-159.

Heinrichs ML, Walker IR, 2006. Fossil midges and palaeosalinity: potential as indicators of hydrological balance and sea-level change. Quat. Sci. Rev. 25:1948-1965.

Hershey AE, 1986. Selective Predation by Procladius in an Arctic Alaskan Lake. Can. J. Fish. Aquat. Sci. 43:2523-2528.

Hill MO, Gauch HG, 1980. Detrended correspondence analysis: An improved ordination technique. Vegetatio 42:47-58.

Hou J, Tian Q, Liang J, Wang M, He Y, 2017. Climatic implications of hydrologic changes in two lake catchments on the central Tibetan Plateau since the last glacial. J. Paleolimnol. 58:257-273.

IPCC, 2007. Climate Change 2007: The Physical Science Basis. Contribution of Working Group I to the Fourth Assessment Report of the Intergovernmental Panel on Climate Change. Cambridge University Press, Cambridge: 996 pp.

IPCC, 2021. Climate Change 2021: The Physical Science Basis. Contribution of Working Group I to the Sixth Assessment Report of the Intergovernmental Panel on Climate Change. Cambridge University Press, Cambridge: 3949 pp.

Jiang L, Nielsen K, Andersen OB, Bauer-Gottwein P, 2017. Monitoring recent lake level variations on the Tibetan Plateau using CryoSat-2 SARIn mode data. J. Hydrol. 544:109-124.

Juggins S, 2014. C2 - Software for ecological and palaeoecological data analysis and visualisation. Version 1.7.7. Newcastle University, Newcastle upon Tyne, UK.

Kasper T, Frenzel P, Haberzettl T, Schwarz A, Daut G, Meschner S, Wang J, Zhu L, Mäusbacher R, 2013. Interplay between redox conditions and hydrological changes in sediments from Lake Nam Co (Tibetan Plateau) during the past 4000cal BP inferred from geochemical and micropaleontological analyses. Palaeogeogr. Palaeoclimatol. Palaeoecol. 392:261-271.

Kasper T, Wang J, Schwalb A, Daut G, Plessen B, Zhu L, Mäusbacher R, Haberzettl T, 2021. Precipitation dynamics on the Tibetan Plateau during the Late Quaternary – Hydroclimatic sedimentary proxies versus lake level variability. Glob. Planet. Change. 205:1-15.

Keil A, Berking J, Mügler I, Schütt B, Schwalb A, Steeb P, 2010. Hydrological and geomorphological basin and catchment characteristics of Lake Nam Co, South-Central Tibet. Quat. Int. 218:118-130.

Kemp AES, 1996. Laminated sediments as palaeo-indicators, p. 7-12. In: AES Kemp (ed.), Palaeoclimatology and Palaeoceanography from Laminated Sediments. Geological Society, London.

Koinig K, Shotky W, Lotter AF, Ohlendorf C, Sturm M, 2003. 9000 years of geochemical evolution of lithogenic major and trace elements in the sediment of an alpine lake - the role of climate, vegetation, and land-use history. J. Paleolimnol. 30:307-320.

Kylander ME, Klaminder J, Wohlfarth B, Löwemark L, 2013. Geochemical responses to paleoclimatic changes in southern Sweden since the late glacial: the Hässeldala Port lake sediment record. J. Paleolimnol. 50:57-70.

Larocque I, 2001. How many chironomid head capsules are enough? A statistical approach to determine sample size for palaeoclimatic reconstructions. Palaeogeogr. Palaeoclimatol. Palaeoecol. 172:133-142.

Last WM, 2002. Tracking environmental change using lake sediments. Kluwer Academic Publishers, Dordrecht: 516 pp.

Laug A, Engels S, Hamerlík L, Turner F, Wang J, Schwalb A, 2018. "Orthocladiinae type K" A special group of chironomid morphotypes from the Tibetan Plateau. Conference Poster in IPA-IAL 2018 Joint Meeting: Unravelling the Past and Future of Lakes, Stockholm.

Laug A, Hamerlík L, Anslan S, Engels S, Turner F, Wang J, Schwalb A, 2019. Acricotopus indet. morphotype incurvatus: Description and genetics of a new Orthocladiinae (Diptera: Chironomidae) larval morphotype from the Tibetan Plateau. Zootaxa 4656:535-544.

Laug A, Schwarz A, Lauterbach S, Engels S, Schwalb A, 2020a. Ecosystem Shifts at two Mid-Holocene Tipping Points in the alpine Lake Son Kol (Kyrgyzstan, Central Asia). Holocene 30:1410-1419.

Laug A, Turner F, Engels S, Wang J, Haberzettl T, Ju J, Yu S, Kou Q, Börner N, Schwalb A, 2020b. Is there a common threshold to subfossil chironomid assemblages at 16 m water depth? Evidence from the Tibetan Plateau. J. Limnol. 79:278-292.

Laug A, Haberzettl T, Pannes A, Schwarz A, Turner F, Wang J, Engels S, Rigterink S, Börner N, Ahlborn M, Ju J, Schwalb A, 2021. Holocene paleoenvironmental change inferred from two sediment cores collected in the Tibetan lake Taro Co. J Paleolimnol 66:171-186.

Lei Y, Yao T, Bird BW, Yang K, Zhai J, Sheng Y, 2013. Coherent lake growth on the central Tibetan Plateau since the 1970s: Characterization and attribution. J. Hydrol. 483:61-67.

Lei Y, Yang K, Wang B, Sheng Y, Bird BW, Zhang G, Tian L, 2014a. Response of inland lake dynamics over the Tibetan Plateau to climate change. Clim. change 125:281-290.

Lei Y, Tian L, Bird BW, Hou J, Ding L, Oimahmadov I, Gadoev M, 2014b. A 2540-year record of moisture variations derived from lacustrine sediment (Sasikul Lake) on the Pamir Plateau. Holocene 24:761-770.

Li L, Yang S, Wang Z, Zhu X, Tang H, 2010. Evidence of Warming and Wetting Climate over the Qinghai-Tibet Plateau. Arct. Antarct. Alp. Res. 42:449-457.

Li M, Kang S, Zhu L, You Q, Zhang Q, Wang J, 2008.

Mineralogy and geochemistry of the Holocene lacustrine sediments in Nam Co, Tibet. Quat. Int. 187:105-116.

Lin Q, Xu L, Hou J, Liu Z, Jeppesen E, Han B-P, 2017. Responses of trophic structure and zooplankton community to salinity and temperature in Tibetan lakes: Implication for the effect of climate warming. Water Res. 124:618-629.

Liu W, Wang L, Chen D, Tu K, Ruan C, Hu Z, 2016. Large-scale circulation classification and its links to observed precipitation in the eastern and central Tibetan Plateau. Clim. Dyn. 46:3481-3497.

Lu C, Yu G, Xi G, 2005. Tibetan Plateau serves as a water tower. Proceedings 2005 IEEE International Geoscience and Remote Sensing Symposium, 2005. IGARSS '05.

Ma N, Szilagyi J, Niu G-Y, Zhang Y, Zhang T, Wang B, Wu Y, 2016. Evaporation variability of Nam Co Lake in the Tibetan Plateau and its role in recent rapid lake expansion. J. Hydrol. 537:27-35.

Ma Y, Lu M, Chen H, Pan M, Hong Y, 2018. Atmospheric moisture transport versus precipitation across the Tibetan Plateau: A mini-review and current challenges. Atmos. Res. 209:50-58.

Mason CF, Bryant RJ, 1974. Periphyton production and grazing by chironomids in Alderfen Broad, Norfolk. Freshwater Biol. 5:271-277.

Meyers PA, Ishiwatari R, 1993. Lacustrine organic geochemistry - an overview of indicators of organic matter sources and diagenesis in lake sediments. Org. Geochem. 20:867-900.

Meyers PA, 2003. Applications of organic geochemistry to paleolimnological reconstructions:a summary of examples from the Laurentian Great Lakes. Org. Geochem. 34:261-289.

Miles J, 2014. Tolerance and variance inflation factor. In: N. Balakrishnan, T. Colton, B. Everitt, W. Piegorsch, F. Ruggeri and J.L. Teugels (eds.), Wiley StatsRef: Statistics Reference Online. J. Wiley & Sons, Chichester.

Moller Pillot HKM, 2013. Chironomidae Larvae, Volume 3: Orthocladiinae. Royal Dutch Natural History Society Foundation Publishing House.

Morrill C, 2004. The influence of Asian summer monsoon variability on the water balance of a Tibetan lake. J. Paleolimnol. 32:273-286.

Morrill C, Overpeck JT, Cole JE, Liu K, Shen C, Tang L, 2006. Holocene variations in the Asian monsoon inferred from the geochemistry of lake sediments in central Tibet. Quat. Res. 65:232-243.

Munsell Color, 2010. Munsell Soil Color Charts: with Genuine Munsell Color Chips. Munsell Color, Grand Rapids.

Nazarova L, Herzschuh U, Wetterich S, Kumke T, Pestryakova L, 2011. Chironomid-based inference models for estimating mean July air temperature and water depth from lakes in Yakutia, northeastern Russia. J. Paleolimnol. 45:57-71.

Nazarova L, Bleibtreu A, Hoff U, Dirksen V, Diekmann B, 2017. Changes in temperature and water depth of a small mountain lake during the past 3000 years in Central Kamchatka reflected by a chironomid record. Quat. Int. 447:46-58.

Nesbitt HW, Fedo CM, Young GM, 1997. Quartz and feldspar stability, steady and non-steady-state weathering, and petrogenesis of siliciclastic sands and muds. J. Geol. 105:173-192.

Oliva P, Viers J, Dupré B, 2003. Chemical weathering in granitic environments. Chem. Geol. 202:225-256.

Phan-Garrigues M, Curton A, Trinh T-H, Schuster M, 2020. Can wind-driven lakes develop in basins with a high rate of sediment supply? A remote sensing based assessment of the lakes of the Tibetan Plateau (Asia). Institute de Physique du Globe de Strasbourg, Ecole et observatoire des sciences de la Terre Université de Strasbourg: 14 pp.

Pu Y, Nace T, Meyers PA, Zhang H, Wang Y, Zhang CL, Shao X, 2013. Paleoclimate changes of the last 1000 yr on the eastern Qinghai–Tibetan Plateau recorded by elemental, isotopic, and molecular organic matter proxies in sediment from glacial Lake Ximencuo. Palaeogeogr. Palaeoclimatol. Palaeoecol. 379-380:39-53.

R Core Team, 2019. R: A language and environment for statistical computing. 1.1.456. R Foundation for Statistical Computing, Vienna.

Ramcharan V, Paterson CG, 1978. A partial analysis of ecological segregation in the chironomid community of a bog lake. Hydrobiologia 58:129-135.

Reimer PJ, Bard E, Bayliss A, Beck JW, Blackwell PG, Ramsex CB, Buch CE, Cheng H, Edwards RL, Friedrich M, Grootes PM, Guilderson TP, Haflidason H, Hajdas I, Hatté C, Heaton TJ, Hoffmann DL, Hogg AG, Hughen KA, Kaiser KF, Kromer B, Manning SW, Niu M, Reimer RW, Richards DA, Scott EM, Southon JR, Staff RA, Turney C, van der Plicht J, 2013. IntCal13 and Marine13 radiocarbon age calibration curves 0-50,000 years cal BP. Radiocarbon 55:1869-1887.

Reimer PJ, Austin WEN, Bard E, Bayliss A, Blackwell PG, Bronk Ramsey C, Butzin M, Cheng H, Edwards RL, Friedrich M, Grootes PM, Guilderson TP, Hajdas I, Heaton TJ, Hogg AG, Hughen KA, Kromer B, Manning SW, Muscheler R, Palmer JG, Pearson C, van der Plicht J, Reimer RW, Richards DA, Scott EM, Southon JR, Turney CSM, Wacker L, Adolphi F, Büntgen U, Capano M, Fahrni SM, Fogtmann-Schulz A, Friedrich R, Köhler P, Kudsk S, Miyake F, Olsen J, Reinig F, Sakamoto M, Sookdeo A, Talamo S, 2020. The IntCal20 Northern Hemisphere radiocarbon age calibration curve (0–55 cal kBP). Radiocarbon 62:725-757.

Schnurrenberger D, Russell J, Kelts K, 2003. Classification of lacustrine sediments based on sedimentary components. J. Paleolimnol. 29:141-154.

Schütt B, Berking J, Frechen M, Frenzel P, Schwalb A, Wrozyna C, 2010. Late Quaternary transition from lacustrine to a fluvio-lacustrine environment in the north-western Nam Co, Tibetan Plateau, China. Quat. Int. 218:104-117.

Sheng E, Yu K, Xu H, Lan J, Liu B, Che S, 2015. Late Holocene Indian summer monsoon precipitation history at Lake Lugu, northwestern Yunnan Province, southwestern China. Palaeogeogr. Palaeoclimatol. Palaeoecol. 438:24-33.

Su F, Duan X, Chen D, Hao Z, Cuo L, 2013. Evaluation of the Global Climate models in the CMIP5 over the Tibetan Plateau. J. Climate 26:3187-3208.

Sun J, Yang K, Guo W, Wang Y, He J, Lu H, 2020. Why Has the Inner Tibetan Plateau become wetter since the mid-1990s? J. Climate 33:8507-8522.

Tarkowska-Kukuryk M, 2014. Spatial distribution of epiphytic chironomid larvae in a shallow macrophyte-dominated lake: effect of macrophyte species and food resources. Limnology 15:141-153.

Ter Braak C, 1987. The analysis of vegetation-environment

relationships by canonical correspondence analysis, p. 69–77. In: I.C. Prentice and E. van der Maarel (eds.), Theory and models in vegetation science. Springer, Dordrecht.

Thompson LG, Mosley-Thompson E, Davis ME, Bolzan JF, Dai J, Klein L, Yao T, Wu X, Xie Z, Gundestrup N, 1989. Holocene-late pleistocene climatic ice core records from Qinghai-Tibetan Plateau. Science 246:474-477.

Thompson LG, Yao T, Davis ME, Henderson A, Mosley-Thompson E, Lin P-N, Beer J, Synal H-A, Cole-Dai J, Bolzan JF, 1997. Tropical climate instability: The last glacial cycle from a Qinghai-Tibetan ice core. Science 276:1821-1825.

Thompson LG, Tandong Y, Davis ME, Mosley-Thompson E, Mashiotta TA, Lin P-N, Mikhalenko VN, Zagorodnov VS, 2006. Holocene climate variability archived in the Puruogangri ice cap on the central Tibetan Plateau. Ann. Glaciol. 43:61-69.

Thompson LG, Yao T, Davis ME, Mosley-Thompson E, Wu G, Porter SE, Xu B, Lin P-N, Wang N, Beaudon E, Duan K, Sierra-Hernández MR, Kenny DV, 2018. Ice core records of climate variability on the Third Pole with emphasis on the Guliya ice cap, western Kunlun Mountains. Quat. Sci. Rev. 188:1-14.

van Hoang L, Clift PD, Schwab AM, Huuse M, Nguyen DA, Zhen S, 2010. Large-scale erosional response of SE Asia to monsoon evolution reconstructed from sedimentary records of the Song Hong-Yinggehai and Qiongdongnan basins, South China Sea, p. 219–244. In: PD Clift, R Tada, and H Zheng (eds.), Monsoon evolution and tectonic–Climate linkage in Asia. Geological Society, London.

Verschuren D, Laird K, Cumming B, 2000a. Rainfall and drought in equatorial east Africa during the past 1,100 years. Nature 403:410-413.

Verschuren D, Tibby J, Sabbe K, Roberts N, 2000b. Effects of depth, salinity, and substrate on the invertebrate community of a fluctuatingtropical lake. Ecology 81:164-182.

Walker IR, 1987. Chironomidae (Diptera) in paleoecology. Quat. Sci. Rev. 6:29-40.

Wan W, Xiao P, Feng X, Li H, Ma R, Duan H, Zhao L, 2014. Monitoring lake changes of Qinghai-Tibetan Plateau over the past 30 years using satellite remote sensing data. Chin. Sci. Bull. 59:1021-1035.

Wang S, Dou H, 1998. Lakes in China. Science Press, Beijing: 598 pp.

Wang B, Bao Q, Hoskins B, Wu G, Liu Y, 2008. Tibetan Plateau warming and precipitation changes in East Asia. Geophys. Res. Lett. 35:2008GL034330.

Wang R, Yang X, Langdon P, Zhang E, 2011. Limnological responses to warming on the Xizang Plateau, Tibet, over the past 200 years. J. Paleolimnol. 45:257-271.

Wang X, Pang G, Yang M, 2018. Precipitation over the Tibetan Plateau during recent decades:a review based on observations and simulations. Int. J. Climatol. 38:1116-1131.

White DS, Miller MF, 2008. Benthic invertebrate activity in lakes:linking present and historical bioturbation patterns. Aquat. Biol. 2:269-277.

Williams WD, Boulton AJ, Taaffe RG, 1990. Salinity as a determinant of salt lake fauna: a question of scale. Hydrobiologia 197:257-266.

Williams DL, Goward S, Arvidson T, 2006. Landsat: Yesterday, today and tomorrow. Photogramm. Eng. Remote Sens. 72:1171-1178.

Wirth SB, Gilli A, Simonneau A, Ariztegui D, Vannière B, Glur L, Chapron E, Magny M, Anselmetti FS, 2013. A 2000 year long seasonal record of floods in the southern European Alps. Geophys. Res. Lett. 40:4025-4029.

Wray RA, Sauro F, 2017. An updated global review of solutional weathering processes and forms in quartz sandstones and quartzites. Earth-Sci. Rev. 171:520-557.

Wrozyna C, Frenzel P, Steeb P, Zhu L, van Geldern R, Mackensen A, Schwalb A, 2010. Stable isotope and ostracode species assemblage evidence for lake level changes of Nam Co, southern Tibet, during the past 600 years. Quat. Int. 212:2-13.

Wu D, Zhou A, Zhang J, Chen J, Li G, Wang Q, Chen L, Madsen D, Abbott M, Cheng B, Chen F, 2020. Temperature-induced dry climate in basins in the northeastern Tibetan Plateau during the early to middle Holocene. Quat. Sci. Rev. 237:106311.

Wulder MA, Loveland TR, Roy DP, Crawford CJ, Masek JG, Woodcock CE, Allen RG, Anderson MC, Belward AS, Cohen WB, Dwyer J, Erb A, Gao F, Griffiths P, Helder D, Hermosilla T, Hipple JD, Hostert P, Hughes MJ, Huntington J, Johnson DM, Kennedy R, Kilic A, Li Z, Lymburner L, McCorkel J, Pahlevan N, Scambos TA, Schaaf C, Schott JR, Sheng Y, Storey J, Vermote E, Vogelmann J, White JC, Wynne RH, Zhu Z, 2019. Current status of Landsat program, science, and applications. Remote Sens. Environ. 225:127-147.

Wünnemann B, Yan D, Andersen N, Riedel F, Zhang Y, Sun Q, Hoelzmann P, 2018. A 14 ka high-resolution δ18O lake record reveals a paradigm shift for the process-based reconstruction of hydroclimate on the northern Tibetan Plateau. Quat. Sci. Rev. 200:65-84.

Xu X, Lu C, Shi X, Gao S, 2008. World water tower: An atmospheric perspective. Geophys. Res. Lett. 35: 2008GL035867.

Yang B, Qin C, Wang J, He M, Melvin TM, Osborn TJ, Briffa KR, 2014b. A 3,500-year tree-ring record of annual precipitation on the northeastern Tibetan Plateau. P. Natl. Acad. Sci USA 111:2903-2908.

Yang K, Ye B, Zhou D, Wu B, Foken T, Qin J, Zhou Z, 2011. Response of hydrological cycle to recent climate changes in the Tibetan Plateau. Clim. Change 109:517-534.

Yang K, Wu H, Qin J, Lin C, Tang W, Chen Y, 2014a. Recent climate changes over the Tibetan Plateau and their impacts on energy and water cycle: A review. Global Planet Change 112:79-91.

Yang R, Zhu L, Wang J, Ju J, Ma Q, Turner F, Guo Y, 2017. Spatiotemporal variations in volume of closed lakes on the Tibetan Plateau and their climatic responses from 1976 to 2013. Clim. Change 140:621-633.

Yang X, Kamenik C, Schmidt R, Wang S, 2003. Diatom-based conductivity and water-level inference models from eastern Tibetan (Qinghai-Xizang) Plateau lakes. J. Paleolimnol. 30:1-19.

Yao T, Shi Y, Thompson LG, 1997. High resolution record of paleoclimate since the Little Ice Age from the tibetan ice cores. Quat. Int. 37:19-23.

Yao T, Masson-Delmotte V, Gao J, Yu W, Yang X, Risi C, Sturm C, Werner M, Zhao H, He Y, Ren W, Tian L, Shi C, Hou S, 2013. A review of climatic controls on δ18O in precipitation

over the Tibetan Plateau: Observations and simulations. Rev. Geophys. 51:525-548.

You Q, Kang S, Aguilar E, Yan Y, 2008. Changes in daily climate extremes in the eastern and central Tibetan Plateau during 1961-2005. J. Geophys. Res. 113:D23107.

You Q, Min J, Kang S, 2016. Rapid warming in the Tibetan Plateau from observations and CMIP5 models in recent decades. Int. J. Climatol. 36:2660-2670.

Yu Z, Wu G, Li F, Huang J, Xiao X, Liu K, 2021. Small-catchment perspective on chemical weathering and its controlling factors in the Nam Co basin, central Tibetan Plateau. J. Hydrol. 598:126315.

Yuan D, Cheng H, Edwards RL, Dykoski CA, Kelly MJ, Zhang M, Qing J, Lin Y, Wang Y, Wu J, Dorale JA, An Z, Cai Y, 2004. Timing, duration, and transitions of the last interglacial Asian monsoon. Science 304:575-578.

Zervas D, Nichols GJ, Hall R, Smyth HR, Lüthje C, Murtagh F, 2009. SedLog:A shareware program for drawing graphic logs and log data manipulation. Comput. Geosci. 35:2151-2159.

Zhang C, Tang Q, Chen D, 2017b. Recent Changes in the Moisture Source of Precipitation over the Tibetan Plateau. J. Climate 30:1807-1819.

Zhang E, Chang J, Cao Y, Tang H, Langdon P, Shulmeister J, Wang R, Yang X, Shen J, 2017c. A chironomid-based mean July temperature inference model from the south-east margin of the Tibetan Plateau, China. Climate Past 13:185-199.

Zhang E, Jones R, Bedford A, Langdon P, Tang H, 2007. A chironomid-based salinity inference model from lakes on the Tibetan Plateau. J. Paleolimnol. 38:477-491.

Zhang E, Tang H, Cao Y, Langdon P, Wang R, Yang X, Shen J, 2013. The effects of soil erosion on chironomid assemblages in Lugu Lake over the past 120 years. Intern. Rev. Hydrobiol. 98:165-172.

Zhang G, Xie H, Kang S, Yi D, Ackley SF, 2011. Monitoring lake level changes on the Tibetan Plateau using ICESat altimetry data (2003-2009). Remote Sens. Environ. 115:1733-1742.

Zhang G, Yao T, Shum CK, Yi S, Yang K, Xie H, Feng W, Bolch T, Wang L, Behrangi A, Zhang H, Wang W, Xiang Y, Yu J, 2017a. Lake volume and groundwater storage variations in Tibetan Plateau's endorheic basin. Geophys. Res. Lett. 44:5550-5560.

Zhang J, Hu Q, Li Y, Li H, Li J, 2021. Area, lake-level and volume variations of typical lakes on the Tibetan Plateau and their response to climate change, 1972–2019. Geo. Spat. Inf. Sci. 24:1-16.

Zhang J, Wang C, Jiang X, Song Z, Xie Z, 2020. Effects of human-induced eutrophication on macroinvertebrate spatiotemporal dynamics in Lake Dianchi, a large shallow plateau lake in China. Environ. Sci. Pollut. Res. 27:13066-13080.

Zhang P, Cheng H, Edwards RL, Chen F, Wang Y, Yang X, Liu J, Tan M, Wang X, Liu J, An C, Dai Z, Zhou J, Zhang D, Jia J, Jin L, Johnson KR, 2008b. A test of climate, sun, and culture relationships from an 1810-year Chinese cave record. Science 322:940-942.

Zhang Q, Kang S, Wang F, Li C, Xu Y, 2008a. Major Ion Geochemistry of Nam Co Lake and its Sources, Tibetan Plateau. Aquat. Geochem. 14:321-336.

Zhang W, Zhou T, Zhang L, 2017d. Wetting and greening Tibetan Plateau in early summer in recent decades. J. Geophys. Res. Atmos. 122:5808-5822.

Zhisheng A, Kutzbach JE, Prell WL, Porter SC, 2001. Evolution of Asian monsoons and phased uplift of the Himalaya-Tibetan plateau since Late Miocene times. Nature 411:62-66.

Zhou S, Kang S, Chen F, Joswiak DR, 2013. Water balance observations reveal significant subsurface water seepage from Lake Nam Co, south-central Tibetan Plateau. J. Hydrol. 491:89-99.